

From DEPARTMENT OF CLINICAL SCIENCE,  
INTERVENTION AND TECHNOLOGY  
Karolinska Institutet, Stockholm, Sweden

# **ELECTRICAL IMPEDANCE OF HUMAN SKIN AND TISSUE ALTERATIONS: MATHEMATICAL MODELING AND MEASUREMENTS**

Ulrik Birgersson



**Karolinska  
Institutet**

Stockholm 2012

All previously published papers were reproduced with permission from the publisher.

Published by Karolinska Institutet. Printed by Universitetsservice-AB

© Ulrik Birgersson, 2012

ISBN: 978-91-7549-019-9

## ABSTRACT

The overall aim of the studies in this thesis is twofold. One is oriented towards calibrating a classifier in differentiating between malignant melanoma and benign nevi of the skin. The other concerns the development of a mathematical model to ascertain the validity of the electrical properties found in literature and to aid in the design and operation of electrodes as well as to broaden the knowledge of the signal distribution in skin.

In the pursuit of calibrating a classifier in the distinction between benign and malignant cutaneous lesions, an international, multicenter, prospective, non-controlled, clinical study is conducted, where a total of 1807 subjects are enrolled. When the observed accuracy, although significant, is found not to be sufficient for the device to be used as a stand-alone decision support tool for the detection of malignant melanoma, the study is put on hold. The study is then re-initiated after hardware updates and redesign of both probe and electrode are implemented.

The resulting classifier demonstrates that EIS can potentially be used as an adjunct diagnostic tool to help clinicians differentiate between benign and malignant cutaneous lesions, although further studies are needed to confirm the validity of the classification algorithm.

In Paper III the literature values of the electrical properties of stratum corneum obtained by Yamamoto et al. are adjusted, and the impact of both the soaking time and sodium chloride concentration of the applied solvent is shown to significantly alter the measured electrical properties. Thereafter, in Paper IV, more realistic median electrical properties of both the stratum corneum and the underlying skin is inverse engineered from experimental measurements on a large cohort of subjects, by using a mathematical model considering the conservation of charge in combination with an optimization algorithm.

Previously it was thought that the electrical impedance of intact skin is dominated by the stratum corneum at low frequencies ( $\leq 1$  kHz) and by the underlying layers at higher frequencies ( $\geq 1$  MHz). In Paper V, it is shown that the stratum corneum heavily dominates the electrical impedance of intact skin up to frequencies of approximately 100kHz, and that the influence of the stratum corneum is not negligible even at 1MHz.

**Key Words:** Electrical impedance, diagnostics, sensitivity and specificity, skin cancer, melanoma, epidermis, dermis, subcutaneous fat, mathematical modeling, optimization, finite element analysis

# LIST OF PUBLICATIONS

This thesis is based on the following publications

- I. P. Åberg, U. Birgersson, P. Elsner, P. Mohr and S. Ollmar, Electrical impedance spectroscopy and the diagnostic accuracy for malignant melanoma. *Exp. Dermatology*. 20 (8), 648-652, 2011
- II. P. Mohr, U. Birgersson, C. Berking, C. Henderson et. al. Electrical Impedance Spectroscopy as a potential adjunct diagnostic tool for cutaneous melanoma. *Skin Res Technol*, accepted on 9/11/2012.
- III. U. Birgersson, E. Birgersson, P. Åberg, I. Nicander and S. Ollmar, Non-invasive bioimpedance of intact skin: mathematical modeling and experiments. *Physiol. Meas*, 32 (1), 1-18, 2011
- IV. U. Birgersson, E. Birgersson, I. Nicander and S. Ollmar. A methodology for extracting the electrical properties of human skin. Submitted to *Physiol. Meas*.
- V. U. Birgersson, E. Birgersson and S. Ollmar. Estimating electrical properties and the thickness of skin with electrical impedance spectroscopy: Mathematical analysis and measurements. *J Electr Bioimp*, 3, pp. 51–60, 2012

# CONTENTS

1	Introduction.....	1
2	Human skin.....	2
2.1	The epidermis .....	2
2.2	The dermis .....	4
2.3	The subcutis .....	4
3	Electrical impedance .....	5
3.1	Electrical impedance of living tissue .....	5
3.2	Skin impedance.....	7
4	Nevi and skin cancer .....	8
4.1	Nevi .....	8
4.2	Malignant melanoma .....	8
4.2.1	Incidence and mortality of malignant melanoma .....	8
4.2.2	Melanoma staging .....	10
4.2.3	Survival.....	11
4.3	Basal cell carcinoma and squamous cell carcinoma.....	12
5	Aims .....	13
6	Material and methods .....	14
6.1	Data analysis process.....	14
6.1.1	Data acquisition .....	14
6.1.2	Data preparation .....	14
6.1.3	Modeling and learning systems .....	14
6.1.4	Verification.....	14
6.1.5	Validation .....	14
6.2	Electrical impedance measurements .....	15
6.2.1	Electrical impedance spectrometer .....	15
6.2.2	Micro-invasive electrode.....	16
6.2.3	Non-invasive electrode.....	17
6.2.4	General examination procedure .....	17
6.2.5	Cancer detection examination procedure .....	17
6.2.6	Skin stripping examination procedure .....	18
6.3	Naked eye examination and dermatoscopy .....	19
6.3.1	Clinical diagnosis .....	21
6.4	Histopathology diagnosis .....	21
6.5	Clinical study design .....	22
6.6	Data collection .....	23
6.7	Data analysis of electrical impedance measurements.....	24
6.7.1	Principle component analysis (PCA).....	24
6.8	Classifiers.....	26
6.8.1	k-nearest neighbors (k-NN) .....	26
6.8.2	Support vector machine (SVM).....	26
6.9	Clinical efficacy endpoints .....	28
6.9.1	Sensitivity and specificity .....	28
6.9.2	ROC – Receiver operating curve .....	28
6.9.3	Safety .....	30
7	Mathematical modeling of skin.....	31

7.1	Introduction.....	31
7.2	Skin composition .....	31
7.3	Electrical impedance electrode .....	32
7.4	Mathematical model .....	32
7.4.1	Governing equations in the transient domain.....	33
7.4.2	Governing equations in the frequency domain .....	34
7.4.3	Boundary conditions .....	34
7.4.4	Constitute relations.....	35
7.5	Analytical solution.....	35
7.6	Model limitations.....	35
8	Results and short discussion .....	36
8.1	Study I.....	36
8.2	Study II .....	38
8.3	Study III.....	40
8.4	Study IV .....	42
8.5	Study V .....	45
9	General discussion and conclusions .....	47
9.1	Efficacy.....	47
9.2	Requirements and consideration for adjunct diagnostic usage .....	48
9.3	Mathematical modeling and electrical properties of skin .....	49
10	Future studies.....	51
10.1	Clinical studies.....	51
11	Acknowledgements .....	52
12	References .....	53

## LIST OF ABBREVIATIONS

AE	Adverse Event
aNN	Artificial Neural Network
AT	Fat
AUC	Area under curve (ROC)
BCC	Basal cell carcinoma
CRO	Contract Research Organisation
DN	Dysplastic Nevus
EIS	Electrical Impedance Spectra
FEM	Finite Element Method
FLD	Fisher Linear Discriminant
FN	False Negative
FP	False Positive
ICH-GCP	Good Clinical Practice (International Conference on Harmonization)
IMATS	International Melanoma Algorithm Training Study
kNN	k Nearest Neighbors
LMM	Lentigo Malignant melanoma
MM	Cutaneous Malignant Melanoma
PAD	Pathologic-Anatomic Diagnosis
PCA	Principal Component Analysis
PLS	Partial Least Squares
ROC	Receiver operating curve
SAE	Serious Adverse Event
SC	Stratum corneum
SCC	Squamous Cell Carcinoma
SK	Sebhorreic keratosis
SSM	Superficial Spreading Melanoma
SVM	Support Vector Machine
TN	True Negative
TP	True Positive
VS	Viable skin (Living Epidermis + Dermis)



# 1 INTRODUCTION

Electrical impedance is the measure of a material's opposition to the flow of alternating electric currents of various frequencies. Electrical impedance of biological materials reflects the clinical status of the tissue under study. In general, impedance at low frequencies is related mainly to the electrical properties of the extra-cellular environments, whereas impedance at high frequencies is related both to the electrical properties of the intra- and extracellular environments and the capacitive properties of the cell membranes. Electrical impedance spectroscopy of biomaterials is reviewed in [1] and for skin specifically in [2].

It has been shown that there are statistically significant electrical impedance differences between reference skin and several lesion types, i.e. basal cell carcinoma (BCC), squamous cell carcinoma (SCC) [3-5]. In preliminary studies [6-8], it was demonstrated that it is possible to use the differences between BCC and benign nevi to identify the lesions with significant diagnostic power. In [7-8] it was demonstrated that impedance measured non-invasively can be used to separate non-melanoma skin cancers (BCCs and SCCs) and actinic keratosis from harmless benign nevi with a high accuracy level, and that it is possible to sort out malignant melanoma from benign nevi albeit with a lower, though clinically relevant, accuracy.

In [9] it was proposed that a new type of micro-invasive electrode furnished with extremely small pins that penetrate into the stratum corneum would reduce the electrical impedance of the stratum corneum, and, consequently, be less influenced by possibly irrelevant biological variations than electrical impedance measured with a non-invasive flat electrode. It was subsequently demonstrated that the accuracy of malignant melanoma detection was higher for the micro-invasive technique than the regular non-invasive [10]. As the proof of principle study for melanoma detection with electrodes furnished with micro spikes only included 16 melanoma, the need for additional studies to both develop and validate the technique was apparent.

In view thereof, the primary aim of this thesis was to carry out two large multicenter studies to develop a classifier to differentiate between benign skin lesions and malignant melanoma and to validate the techniques safety and effectiveness.

During the course of the development it became apparent that the electrical properties of skin found in literature were unable to accurately predict the experimental findings and thus part of the thesis work became oriented towards mathematical modeling and experiments to enable the extraction of more realistic electrical properties for skin.

## 2 HUMAN SKIN

The human skin is a complex organ that covers the exterior of the body. It is the single largest human organ both by sheer weight and surface area. It comprised three main layers: epidermis, dermis and subcutis as depicted in Figure 1.

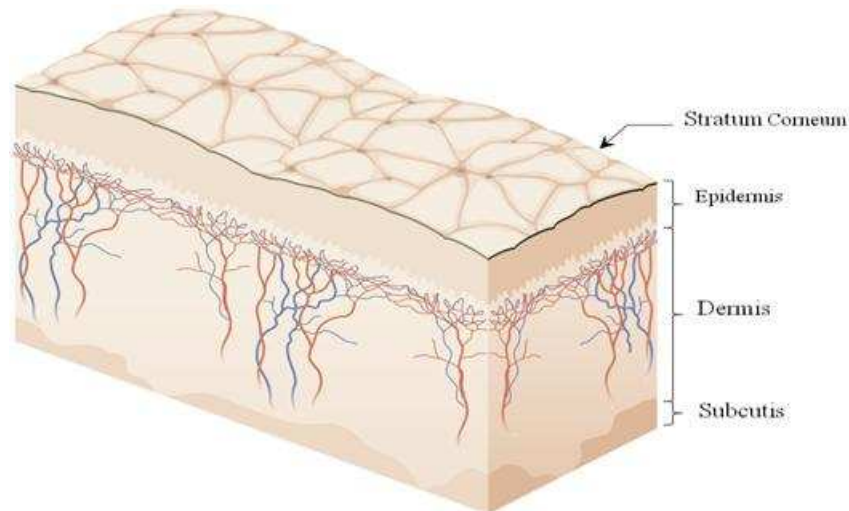


Figure 1 – Cross section of the skin.

The outermost layer, the epidermis, acts as a barrier against radiation, chemicals and pathogens whilst limiting water loss through the skin. Between the epidermis and subcutis lies the dermis, whose main function is to supply the epidermis with nutrients and to provide both mechanical strength and elasticity. The innermost layer, the subcutis, consists mainly of fat and loose connective tissue and functions as an insulator and shock absorber.

A literal interpretation of the word subcutis, meaning beneath the skin, will imply that the skin encompasses only two layers. However, given the interaction and functionality of the subcutis with the epidermis and dermis, a pragmatic approach is to see it as an integral part of the skin [11-12].

### 2.1 THE EPIDERMIS

The epidermis is composed mainly of keratinocytes. The innermost layer (stratum germinativum) consists mainly of strictly ordered basal cells where approximately every tenth cell is interchanged with a melanocyte, pigment producing cell. It is anchored to the basement membrane at the epidermal-dermal junction. The basal cells actively differentiate, some of which migrate towards the surface of the skin slowly becoming more and more flattened anucleate plates of keratin (keras meaning horn), which can be found in the outermost layer (stratum corneum or horny layer). An especially important protective role can be constituted to the melanocyte. By producing melanin granules (small pigmented particles) UV radiation can efficiently be absorbed and transformed into heat [13], thereby protecting the DNA from the damaging effects

of the UV radiation which, to a large extent, is attributed to the formation of malignant melanoma and other skin cancers.

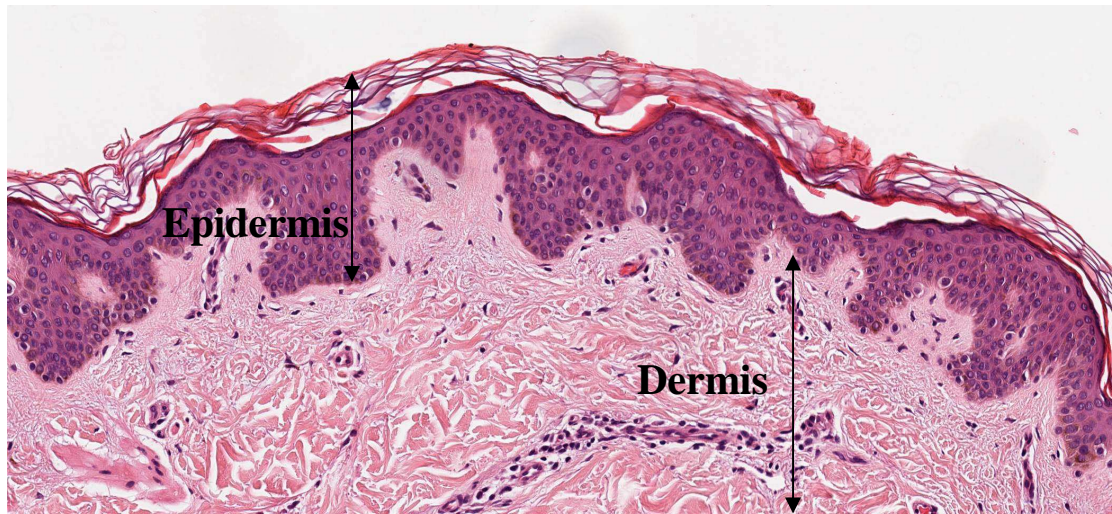


Figure 2 – Epidermis and part of dermis

In between the basal and corneum strata (layer), two cell transitional stages can be found, the spinous and granular cell layer. In the spinosum strata, the cells start to shrink, although they still remain tightly packed through the high number of cell-to-cell cohesion proteins (desmosomes). It is within these spinous cells the keratin is formed. In the subsequent layer, the stratum granulosum, the cells flatten substantially and lose their cell organelles including their nuclei. A histology section of the epidermis stained with hematoxylin and eosin, as seen under the microscope, is illustrated in Figure 2

Depending on body site, the epidermal skin thickness varies considerably between 0.1 mm up to 2 mm [14]. The variation in epidermal skin thickness is almost completely due to the variation in the stratum corneum thickness, where it is approximately 10-20  $\mu\text{m}$  thick in general it can be as thick as 2 mm on the palms of the hands and feet, as illustrated in Figure 3.

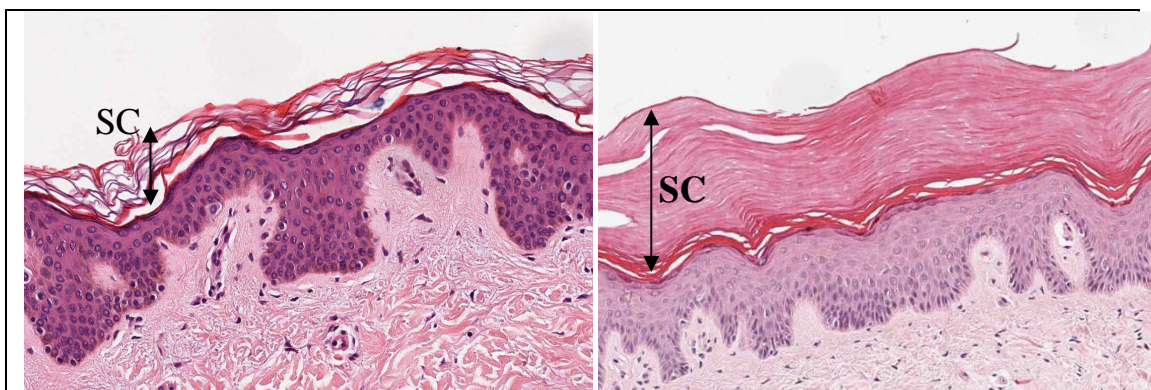


Figure 3 – Stratum Corneum (SC) thickness (a) upper back and (b) palm of sole

Within the epidermis, other cellular components can be found such as the Langerhans' cells, which forms part of the body's immune system, and Merkel cells being specialized nerve endings.

## **2.2 THE DERMIS**

Directly underneath the epidermis lies the skin's thickest layer, the dermis. It consists mainly of collagen and elastin fibers intricately woven into a matrix providing the skin with mechanical strength and elasticity. It is divided into 2 sub-layers of varying thickness: the papillary and reticular dermis. The papillary dermis situated directly underneath the basement membrane intertwines with the rete-ridges of the epidermis in a papillary (nipple-like) formation to increase the exchange of nutrients and metabolites between the two layers. The thicker reticular dermis underneath has a higher concentration of coarser collagen and elastin fiber bundles.

Within the dermis a large number of other cellular components can be found:

- fibroblasts responsible for manufacturing collagen,
- mast cells involved in moderating immune and inflammatory processes,
- macrophages having a central role in the immune system,
- sweat glands involved in the temperature regulation
- hair follicles,
- sebaceous glands,
- sensory receptors and
- blood vessels.

## **2.3 THE SUBCUTIS**

The subcutis, found underneath the dermis (except for the scrotum where no subcutis is present), mainly consists of lipocytes, which are specialized fat storing cells and some loose connective tissue. Due to the high percentage of fat in this layer, it is often referred to as the subcutaneous fat and thereby functions as a good insulator and shock absorber. Its thickness varies depending on anatomical site, nutritional and hormonal status in conjunction with many other factors.

Other cellular components found in this layer are nerves and blood vessels.

### 3 ELECTRICAL IMPEDANCE

Electrical impedance is a measure of a material's opposition to the flow of alternating electric currents of various frequencies. Electrical impedance of biological materials reflects the clinical status of the tissue under study. Normal and abnormal tissue differ with regards to cell size, shape, orientation, compactness, and structure of cell membranes, as illustrated in Figure 4. These different properties influence the ability of the tissue to conduct and store electricity. This means that the properties also will be reflected in an EIS measurement. A tissue alteration that would be discovered in a microscope during a traditional, histological examination can also be seen as an imprint in the impedance spectrum.

In general, impedance at low frequencies is related mainly to the resistive properties of the extra-cellular environments, whereas impedance at high frequencies is related both to the resistive properties of the intra- and extra-cellular environments and the capacitive properties (reactance) of the cell membranes. The outcome of an EIS measurement is both magnitude and phase shift at each frequency included in the spectrum.

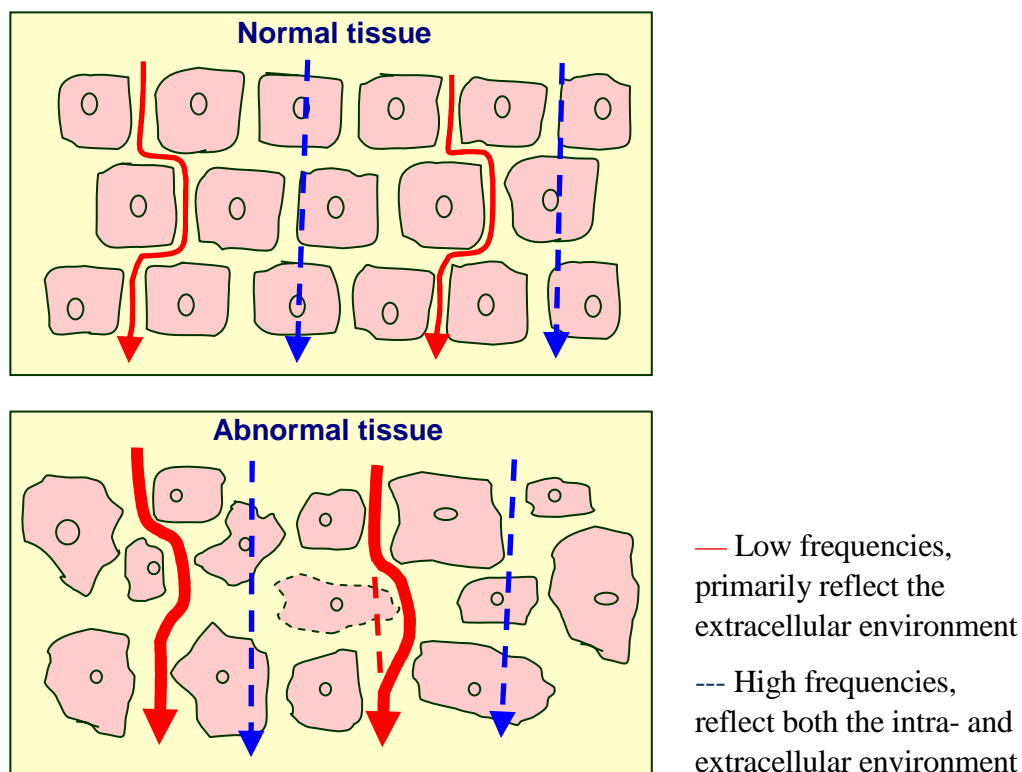


Figure 4 –Illustration of current pathways of low and high frequencies.

#### 3.1 ELECTRICAL IMPEDANCE OF LIVING TISSUE

Electrical impedance of living tissue generally contains three major frequency regions where the electrical impedance decreases with increasing frequency separated by regions with almost constant electrical impedance, as can be seen in Figure 5.

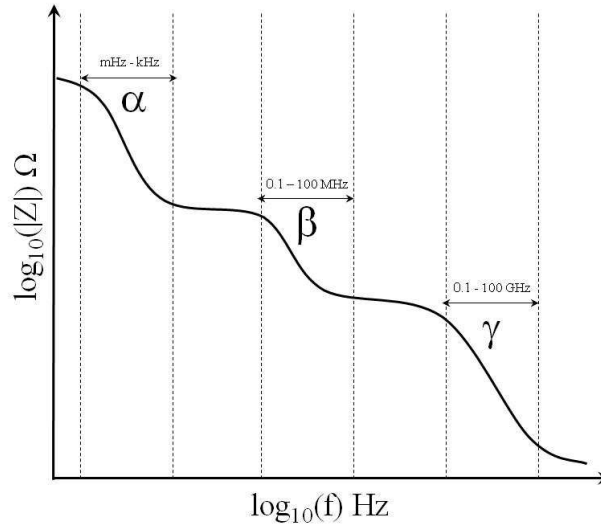


Figure 5 – Schematic of general dispersion regions for living tissue.

These three major regions, where the electrical impedance decreases, are coupled with specific electrochemical mechanisms and are often referred to as dielectric dispersions. The first to identify the three major dispersions, referred to as  $\alpha$ ,  $\beta$  and  $\gamma$ -dispersions, was H.P Schwan [15], as early as 1957. The  $\alpha$ -dispersion found in the characteristic frequency region between mHz up to a few kHz generally reflects the polarization phenomena of ionic clouds near the membrane surfaces. The  $\beta$ -dispersion, found in the frequency region between a few kHz and hundreds of MHz, is related to the polarization effects and structural changes of the cell membranes as well as oedema. The  $\gamma$ -dispersion, in the region between hundreds of MHz to several GHz, is affected by dipolar mechanisms in the relaxation of small polar molecules, in particular water. In conjunction with each dispersion there are sub-dispersions (e.g.  $\alpha_1, \alpha_2, \dots$ ), which can easily be overlooked if the data is fitted to some a priori idea on how the measurements ought to look, such as the Cole-Cole model [16]. This is due to the fact that electrical impedance consists of both a real and imaginary part or, equivalently, the magnitude and the phase shift and curve-fitting to partial data will always filter out a large amount of data, which might just be essential to describe the full extent of the phenomena to be observed. As the frequency intervals imply the dispersions are not always clearly separated and might sometimes overlap. For skin stripped 90 times with cellulose tape, the  $\alpha$  and  $\beta$  dispersions clearly overlap, as can be seen in Figure 6. Foster and Schwan published a thorough review of the electrical properties of tissue [17], Gabrielle et. al. [18] measured and estimated the electrical properties for a large number of tissue types, which have to a large extent been discussed in a pedagogical way in Bioimpedance and Bioelectrical Basics [1] in conjunction with a broad range of electrical impedance applications.

Electrical impedance has been used in a wide range of clinical applications, ranging from differentiation different cancer types [3-10, 19-24], tomography [25] and body composition [26].

### 3.2 SKIN IMPEDANCE

The average electrical properties of stratum corneum and the viable skin underneath were first estimated by Yamamoto & Yamamoto in 1976 [27] by adjusting a tissue circuit equivalent to reflect the measured electrical impedance after applying an 18% sodium chloride solution for 30 minutes before and after stratum corneum stripping, thereby enabling the measurement of the stratum corneum and viable skin respectively. In 1984 Ackmann & Seitz [28] showed that the electrical impedance of intact skin is dominated by the stratum corneum at low frequencies ( $\lesssim 1$  kHz) and by the underlying layers at higher frequencies ( $\gtrsim 1$  MHz). This was clearly confirmed in a computational study conducted in 1999 by Martinsen et al. [29]. Later, Birgersson et al. adjusted the electrical properties of stratum corneum obtained by Yamamoto et al. unmistakably showing that the soaking time and sodium chloride concentration of the applied solvent significantly changes the measured electrical properties [30]. Thereafter, Birgersson et al used a mathematical model considering the conservation of charge in combination with an optimization algorithm to inverse engineer more realistic median electrical properties of both the stratum corneum and the underlying skin from experimental measurements on a large cohort of subjects .[31]. In 2012 Birgersson et al showed that the stratum heavily dominates the electrical impedance of intact skin up to frequencies of approximately 100kHz and that the influence of the stratum corneum is not negligible even at 1MHz [32].

An example of the electrical impedance distribution between the stratum cornum and the underlying skin layers can be shown by measuring the electrical impedance during a tape stripping experiment, as illustrated in Figure 6.

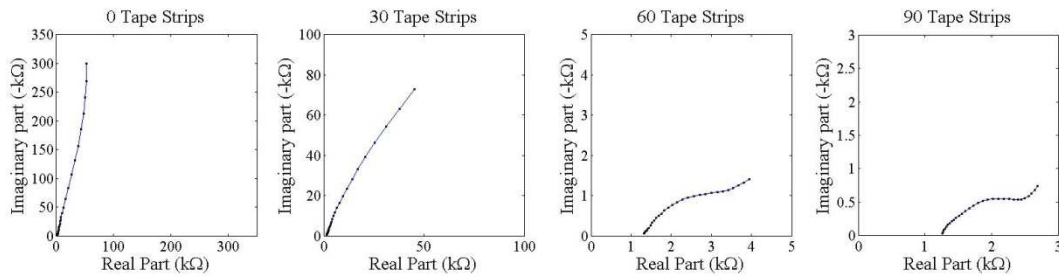


Figure 6 – Nyquist plots of the electrical impedance spectra (frequency range 1.22 kHz to 1 MHz), before tape stripping, and after 30, 60 and 90 tape strips. Note axis scales.

The electrical impedance of skin has been utilized to quantify, assess and characterize skin reactions and diseases [33-40].

## **4 NEVI AND SKIN CANCER**

### **4.1 NEVI**

When an abundance of melanin is present on a specific spot of the skin, these areas are often referred to as moles, spots or pigmented nevi.

During the course of time, these pigmented nevi have been characterized into a large amount of subtypes. For the sake of ease, the pigmented nevi are often categorized in regards to the degree of atypia (abnormality) present in them, which has been correlated to an increased likelihood of progression into malignant melanoma [41-42]. This generates the following classes:

- benign (harmless) pigmented nevi, which are very common
- dysplastic (difficult formation) nevi of mild/moderate/severe atypia
- malignant (harmful) melanoma
- other (both benign and malignant)

Since the skin is composed of many different cells types, other nevi or lesions can form due to an increased growth of other skin cells.

### **4.2 MALIGNANT MELANOMA**

Malignant melanoma arises when melanocytes start to grow uncontrollably, due to a specific mutation in the DNA structure. Most cases of cell mutation leads to programmed cell death (apoptosis) except when a very small set of genes, called oncogenes are mutated, in which case the cell can start to proliferate uncontrollably (cancer). In most cases, a mutated oncogene often requires an additional transformation prior to developing into the state of uncontrollable proliferation, such as a mutation in another gene or a viral infection. If the cancer is left untreated it can start to spread via blood and lymph vessels to the lymph nodes, other organs or other distant tissues (metastasis).

The transformation from a benign into a malignant melanocyte is not yet fully understood, but sun exposure especially in early childhood and sunburns in people with fair/white skin seem to be important risk factors, which clearly is reflected in the melanoma incidence and mortality in the following section. Since melanoma also do arise in sun-protected areas (such as in the mouth, genitalia and under eyelids), sun exposure is not the only risk factor for developing melanoma. Some other risk factors that need to be taken into account are family history of melanoma, previous melanoma, large number of melanocytic (pigmented) nevi, skin color/type, genetic disposition as well as other environmental factors [41-52].

#### **4.2.1 Incidence and mortality of malignant melanoma**

Melanoma incidence has increased more than 3-fold since 1980, and if current trends continue, it has been estimated that 1 of every 75 people born in US during 2000 will

develop melanoma [53]. Melanoma incidence rates are by far highest in countries having a sun exposed and fair-skinned population, as can be seen in Figure 7.

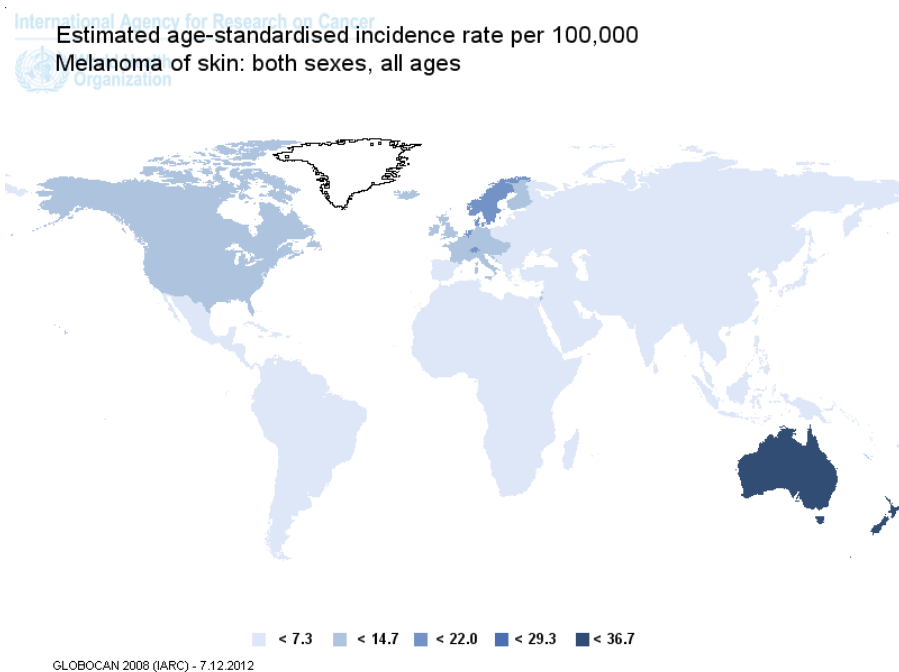


Figure 7 – The incidence of melanoma in the world [54].

Countries in the developed world account for the major part of all malignant melanoma cases with approximately 200000 new diagnosed cases in 2010, where Europe accounted for 52%, US 39% and Australia/New Zealand for the remaining 9% [54].

As with incidence rates, the mortality rates are highest in countries having a fair-skinned population, as can be inferred from Figure 8. Approximately 46000 died in developed countries during 2010 due to late stage melanoma [54].

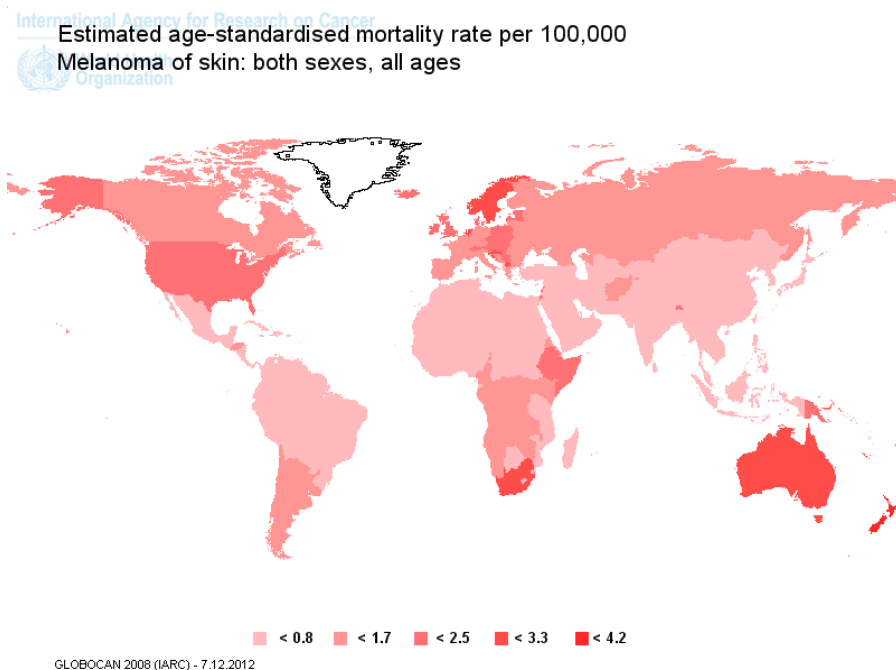


Figure 8 – The mortality of melanoma in the world [54].

### 4.2.2 Melanoma staging

All cancers are staged according to the **Thickness Nodular Metastasis (TNM)** classification [55]. The primary tumor thickness (**T**) is measured, the regional lymph nodes checked for presence of tumor cells (**Regional Lymph Nodes**) and whether the tumor has spread to other organs or distant tissues (**Distant Metastasis**).

For melanoma the tumor is then graded into different categories in accordance to the TNM classification [55] as depicted in Table 1.

Table 1. Melanoma TNM Classification [55]

Primary Tumor Thickness (T)		
T Classification	Thickness	Ulceration Status
Tx	Cannot be assessed (curettage (scraping or scooping) or fully regressed melanoma)	N/A
T0	No Evidence of primary tumor	
Tis Melanoma in situ (in place)	N/A	N/A
T1*	≤ 1.0mm	a: w/o ulceration and mitosis < 1 / mm2 b: with ulceration and mitosis ≥ 1 / mm2
T2	1.01-2.0mm	a: w/o ulceration b: with ulceration
T3	2.01-4.0mm	a: w/o ulceration b: with ulceration
T4	> 4.0mm	a: w/o ulceration b: with ulceration
Regional Lymph Nodes (N)		
N Classification	# of Metastatic Nodes	Nodal Metastatic Mass
N0	No evidence of lymph node metastasis	
N1	1 node	a: micrometastasis b: macrometastasis
N2	2-3 nodes	a: micrometastasis b: macrometastasis c: In transit mestases/satellites without metastatic nodes
N3	4 or more metastatic nodes, or matted nodes, or in-transit metastases/satellites and metastatic nodes	
Distant Metastasis (M)		
M Classification	Site	Serum LDH
M0	No evidence of metastasis to distant tissues or organs	
M1a	Distant skin, subcutaneous or nodal metastases	Normal
M1b	Lung metastases	Normal
M1c	All other visceral metastases	Normal

	Or any distant metastases	Elevated
--	---------------------------	----------

\* The use of mitotic rate to differentiate between T1a and T1b is not yet part of standard care in all countries, e.g. Sweden has not established this as part of the diagnosis yet.

By combining the TNM classes a clinical staging of melanoma can be conducted as given in Table 2. This helps in determining the appropriate treatment and survival of the patient.

Table 2. Clinical staging of malignant melanoma [55]

<b>Clinical Staging</b>			
Stage 0	Tis	N0	M0
Stage IA	T1a	N0	M0
Stage IB	T1b	N0	M0
	T2a	N0	M0
Stage IIA	T2b	N0	M0
	T3a	N0	M0
Stage IIB	T3b	N0	M0
	T4a	N0	M0
Stage IIC	T4b	N0	M0
Stage III	Any T	≥N1	N0
Stage IV	Any T	Any N	M1

### 4.2.3 Survival

As with all cancers, survival generally decreases drastically with increasing tumor thickness and whether the tumor has metastasized. For melanoma, the 10-year survivability can be categorized in accordance with the measured Breslow thickness (T-class) as depicted in

Table 3 as well as according to the clinical staging, taking the thickness and metastatic potential in consideration as shown in Figure 9.

Table 3. Melanoma Classification according to Primary Tumor Thickness [55]

<b>Thickness</b>	<b>10-year survival</b>
Tis	~100%
T1	92%
T2	80%
T3	63%
T4	50%

Where thin melanomas can be considered cured with only surgical excision, a thick melanoma has a very low 5-year survival and metastatic melanoma (Stage IV melanoma) of any thickness has an extremely poor 5-year survival [56], due to the solemn fact that there is still no efficient treatment for metastatic melanoma. Therefore, early detection of malignant melanoma is vital for treatment outcome and survival rate.

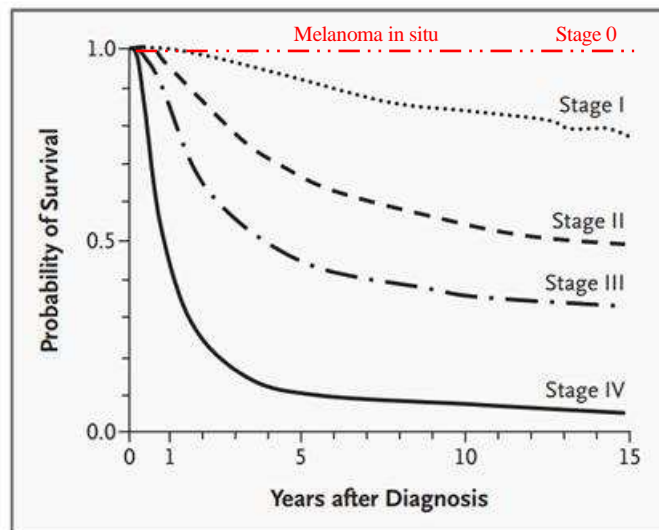


Figure 9 – Kaplan-Meier survival curves for the relationship between stage of melanoma and survival [56] with addition of Stage 0.

### 4.3 BASAL CELL CARCINOMA AND SQUAMOUS CELL CARCINOMA

If the basal cells or the spindle cells undergo a mutation of the oncogenes, then either a basal cell carcinoma or a squamous cell carcinoma may develop. These skin cancers are generally referred to as non-melanoma skin cancers. Even though the incidence of basal cell carcinoma is over 10 times as frequent as melanoma, the mortality is extremely low as they very rarely metastasize. Squamous cell carcinoma is 1.5 times as frequent as melanoma, they sometimes do metastasize, but they are not as malignant as melanoma. The choice of treatment depends on a number of factors such as tumor size, type, thickness, localization and patient age and can involve surgical excision, curettage, topical creams as well as other forms of treatment [57-58].

## 5 AIMS

The overall aim of the studies in this thesis is twofold. The first, to calibrate a classifier able to differentiate between malignant melanoma and benign nevi of the skin. The other, concerns the development of a mathematical model to ascertain the validity of the electrical properties found in literature and to aid in the design and operation of electrodes as well as to broaden the knowledge of the signal distribution in skin.

This thesis is based on five papers with the following specific aims:

- I. To investigate the accuracy of electrical impedance spectroscopy in distinguishing between malignant melanomas and benign skin lesions using an automated classifier.
- II. To develop a classification algorithm to distinguish between melanoma and benign lesions of the skin with sensitivity above 98% and specificity approximately 20 percentage points higher than the participating study dermatologists.
- III. To derive a mathematical model considering conservation of charge in the various layers of the skin and adjacent electrodes as well as validating the model with experimental findings.
- IV. To introduce and validate a new methodology allowing for efficient determination of the electrical properties of skin for arbitrary conditions (within limits) and to extract more realistic electrical properties for the stratum corneum and viable skin than are currently found in literature.
- V. To (i) explore electrical impedance spectroscopy (EIS) as an alternative technique for estimating the stratum corneum thickness, (ii) secure closed-form analytical solutions for our earlier mathematical model of EIS from Paper IV (iii) verify the analytical solutions with the full model and validate both with further experimental measurements, and (iv) estimate the stratum corneum thickness and its associated electrical properties that are key for EIS.

## **6 MATERIAL AND METHODS**

### **6.1 DATA ANALYSIS PROCESS**

The data analysis process entails problem understanding, data acquisition, data preparation, modeling, evaluation, verification and validation.

In the following, a brief introduction to each step is given and the numerical tools employed.

#### **6.1.1 Data acquisition**

This step is generally the most tedious and time consuming part, but should not be overlooked as it is vital to gather data that not only is relevant, but spans the whole problem domain. As brief insight, it took 5 years to gather sufficient amount of nevi in the international melanoma trials to enable the calibration of a classifier. A large part of that time was spent on adjusting the inclusion criteria and upgrading the system to reduce operator dependency, increase the signal to noise ratio and migrating from a silicon spiked electrode to an electrode furnished with micro-invasive spikes based on plastic.

#### **6.1.2 Data preparation**

Once the data is collected, the first step is to clean the data from inaccuracies that have occurred during the acquisition phase, such as general data errors, noise and outliers. First thereafter the data may be grouped, transformed, scaled, re-sampled and reduced in dimensionality. Once all data has been preprocessed, it can finally be merged into one single dataset for modeling purposes.

#### **6.1.3 Modeling and learning systems**

There are numerous models and learning systems that can be employed to solve a specific problem, but quite often the exact type is not critical, provided the data acquisition and preparation phase has turned the data into something sensible. A couple of different classifiers are exemplified in section 6.8.

#### **6.1.4 Verification**

Verification is intended to determine whether or not a model meets the given requirements and specifications prior to having a totally independent dataset that encompasses the problem domain. Most often during development of a model, one is faced with not having sufficient data to ensure its full validity and therefore different methods such as cross-validation to test the accuracy and robustness of the solution are employed.

#### **6.1.5 Validation**

Validation occurs when model performance is tested on a dataset that is independent from the dataset used for calibration purposes. This may of course be part of the data

acquisition phase, but to acquire data for both calibration and validation purposes might not only be cumbersome but very time-consuming and costly.

## 6.2 ELECTRICAL IMPEDANCE MEASUREMENTS

### 6.2.1 Electrical impedance spectrometer

Throughout the data acquisition phase, three different electrical impedance spectrometers have been used with almost equivalent modes of operation, therefore only the latest electrical impedance spectrometer will be described. The interested reader is referred to earlier publications [40, 59] or to SciBase [60] for further information.

The electrical impedance spectrometer, SciBase III, consists of a control unit, a measurement probe and a disposable micro invasive electrode as shown in Figure 10. The control unit, connected with the mains through a power cord with 110/240 V, processes examination data and presents the results of the EIS measurement on the display. The display is equipped with a touch screen for user interaction. The probe unit, connected to the control unit through a cable, is used to initiate the electrical impedance measurements by pressing down its movable spring loaded probe housing.

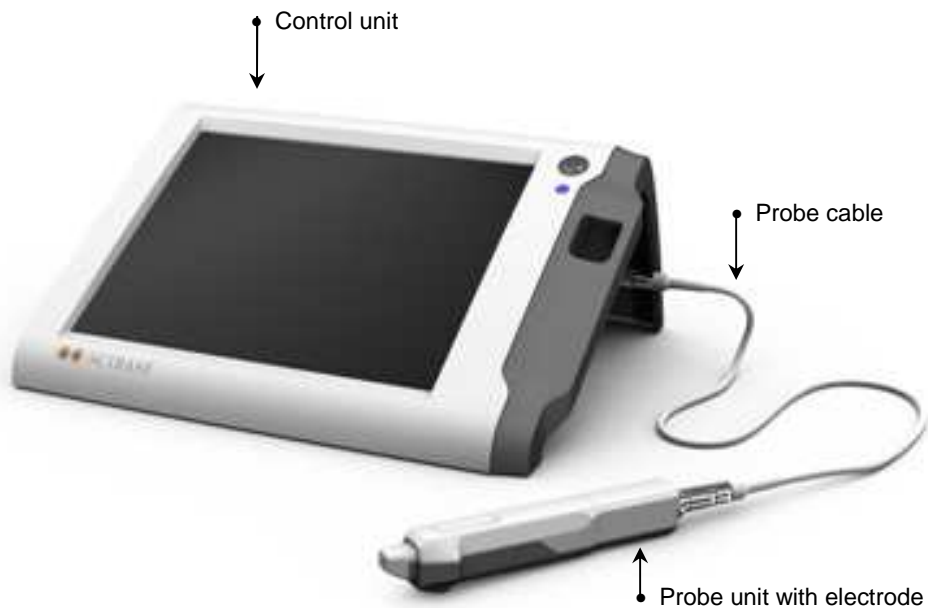


Figure 10 – SciBase III system

The system measures electrical impedance at 35 set frequencies, logarithmically distributed from 1.0 kHz to 2.5 MHz. A complete electrical impedance measurement takes less than 10 s. The applied voltage and resulting current is limited to 150mV and 75 $\mu$ A respectively. This results in a maximum of power and energy that can be delivered to the skin tissue of 11.25 $\mu$ W and 113 $\mu$ J respectively. Since it takes 4.186 Joule to heat 1 kilogram or 1 litre of water by 1 degree Celsius, 113 $\mu$ J would therefore be the energy equivalent to heating 1 litre by  $2.7 \times 10^{-8}$  degrees Celsius.

### 6.2.2 Micro-invasive electrode

During an examination the disposable electrode is attached to the probe. It consists of five electrode bars as shown in Figure 11. The surface of each electrode bar is covered with small micro invasive pins covered with gold. The pins are of triangular shape approximately 150  $\mu\text{m}$  high with a 170  $\mu\text{m}$  triangular base. The total area of the electrode is approximately 5 x 5 mm<sup>2</sup>. The pins are designed to penetrate into stratum corneum (approximately 10-20  $\mu\text{m}$  thick).

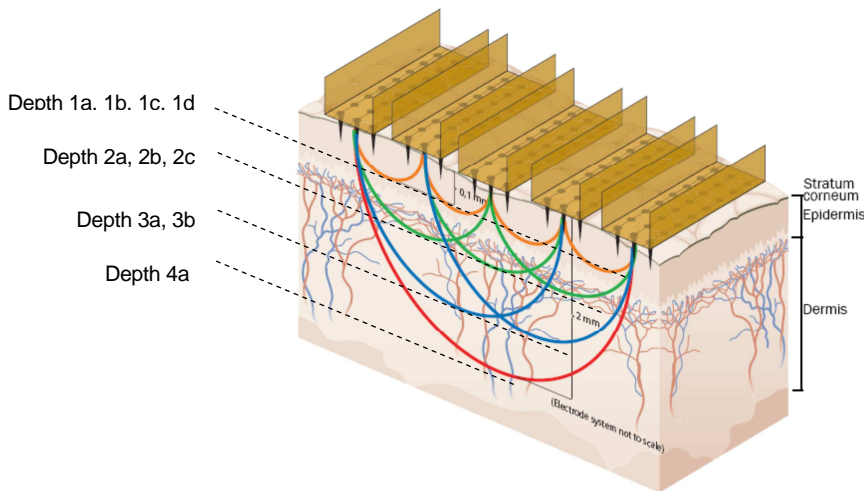


Figure 11 – Depth settings

A scanning electron micrograph of the pins is shown in Figure 12. Since the pins neither reach the blood vessels nor the sensory nerves in the dermis, the probe is classified as micro-invasive. Measurements with the electrodes are painless. The electrode is for single-patient use. After an examination, the operator removes the electrode and disposes of it.

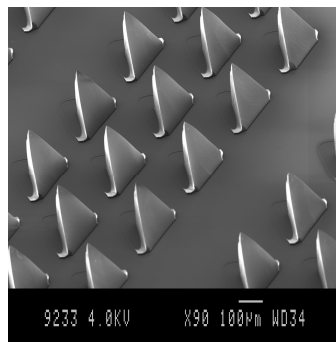


Figure 12 – Electron micrograph of the micro-pins on the surface of the electrode system. The pins are 150  $\mu\text{m}$  long with a 170  $\mu\text{m}$  triangular base

When the disposable micro-invasive electrode is attached to the system it measures at four different depths and 10 set permutations, as illustrated in Fig x. The depth selectivity is facilitated by the use of one sense and one injection electrode. It is the spatial localisation of the sense and injection electrode that determines the depth penetration, as can be seen in Figure 11.

### 6.2.3 Non-invasive electrode

The system can also be equipped with a non-disposable flat concentric electrode system, as depicted in Figure 13. The non-invasive probe was designed so that two-point measurements can be carried out to 5 depth settings; for this purpose, the probe features two voltage injection electrodes, one current detector and a guard electrode to decrease the impact of surface leakage currents [59]. The electrical impedance is given by a measured magnitude (kohms) and a phase shift (degrees) at five different current penetrations depths resulting from varying the voltage at the second injection electrode from 5 to 50 mV whilst keeping the voltage constant at 50 mV at the primary injection electrode.

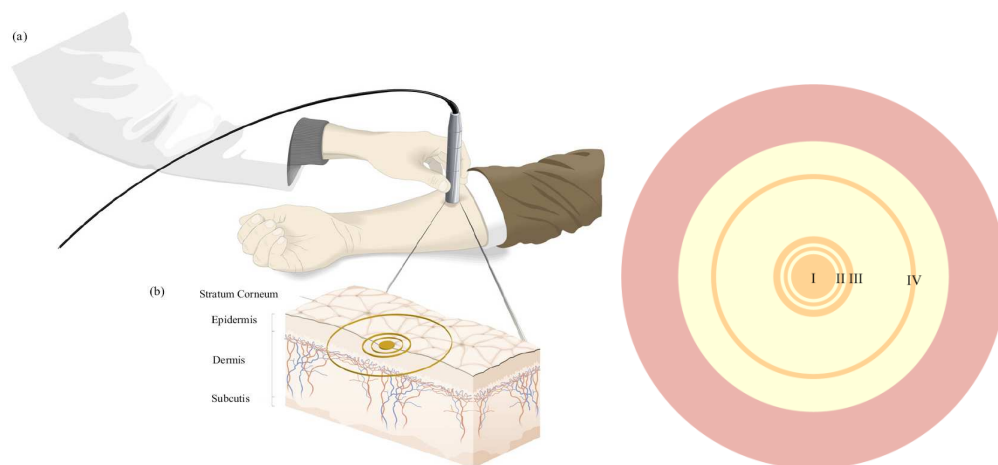


Figure 13 – Schematic overview of the concentric electrodes are marked as (I) current detection, (II) guard, (III) secondary inject and (IV) primary injection.

### 6.2.4 General examination procedure

Prior to measurements, the skin site is soaked with physiological saline solution (0.9 % salt concentration) for a minimum of 30 seconds (micro-invasive electrode) or 60 seconds (non-invasive electrode). Thereafter the excess fluid is wiped off with a clean and dry compress. The electrode is placed against the skin and a measurement is initiated. The outcome of the measurement is curves of magnitude (in kOhms) and phase shift (degrees) at varying depths and permutations depending on the attached electrode.

### 6.2.5 Cancer detection examination procedure

Electrical impedance measurements are performed after entering patient data into the control unit via the touch screen. The operator will perform at least 2 measurements, one on typical background skin (reference) located ipsi-laterally or contra-laterally to the lesion and one or more on the lesion. Multiple measurements are conducted if needed to cover the whole lesion. Prior to measurements, the skin site is soaked with physiological saline solution (0.9 % salt concentration) for a minimum of 30 seconds. By measuring the typical background skin, reference measurement, the patient becomes its own reference. The outcome of the measurements are curves of magnitude (kOhms, left y-axis) and phase shift (degrees, right y-axis) at four different depths (different

colors) and 10 permutations at various frequencies (x-axis). Examples of curves for measurements of benign nevus with reference measurement (Figure 14) and measurements of malignant melanoma with reference measurement (Figure 15) are provided below.

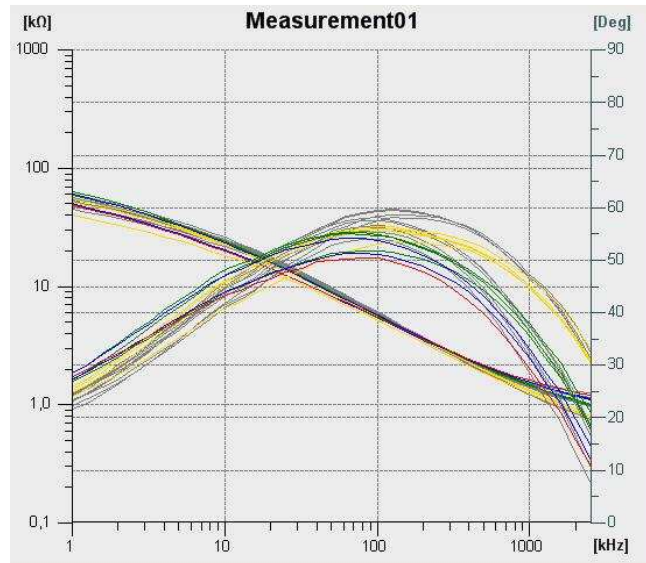


Figure 14 — Benign Nevus - Reference registration (grey) and lesion registration (colored).

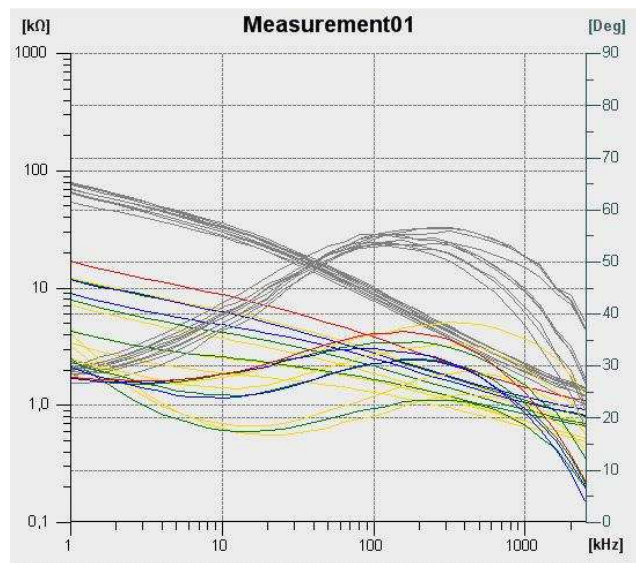


Figure 15 — Malignant Melanoma - Reference registration (grey) and lesion registration (colored).

#### 6.2.6 Skin stripping examination procedure (not part of MM study)

Prior to initiating the skin stripping procedure, an initial measurement on intact skin is performed to establish the subject baseline impedance. Thereafter, Scotch® Magic™ Cellulose Tape is applied on the volar forearm of the subject and removed with a quick snatch. After every fifth consecutive skin stripping an electrical impedance measurement was carried out. This procedure was repeated until a total of 90 stratum-corneum strippings had been performed.


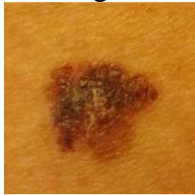
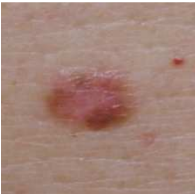

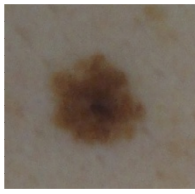

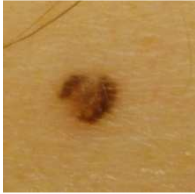

### 6.3 NAKED EYE EXAMINATION AND DERMATOSCOPY

"Malignant melanoma writes its message in the skin with its own ink and it is there for all of us to see. Some see, but do not comprehend." Dr Neville Davis [61]

To help in the comprehension of differentiation of benign pigmented nevi from melanoma, a number of features coupled with an increased risk of melanoma have been derived and are highlighted below.

Today the clinical diagnosis of melanoma is primarily based on a naked eye examination of patients' lesions in combination with family history. The physician assesses each lesion using the well-established ABCD- criteria with the new addition of E. The ABCDE abbreviations stand for **A**symmetry, **B**order Irregularity, **C**olor Variation, **D**iameter greater than 6 mm and **E**volving lesion characterized by changes over time. Examples of lesions showing either no signs or signs of ABCD are depicted in Table 4.

Table 4. Examples of pigmented nevi categorized according to ABCD.

Criteria	Benign	Malignant
A. Asymmetric of the skin lesion	 Symmetrical	 Asymmetrical
B. Border of the skin lesion	 Even Borders	 Uneven Borders
C. Color of the skin lesion	 One shade	 Two or more shades
D. Diameter of the skin lesion	 ≤ 6 mm	 > 6 mm

All lesions shown in the table are taken from the SciBase International Melanoma Pivotal Trial.

In addition to ABCDE criteria, there are a handful of criteria the physician will use to make a decision whether to excise the lesion or not [62]. All lesions the physician finds suspicious will be excised and sent on to histopathology to confirm a diagnosis.

Apply the ABCD rules to the lesions found in Figure 16 and try to find the melanoma. Note, there might just be more than one.

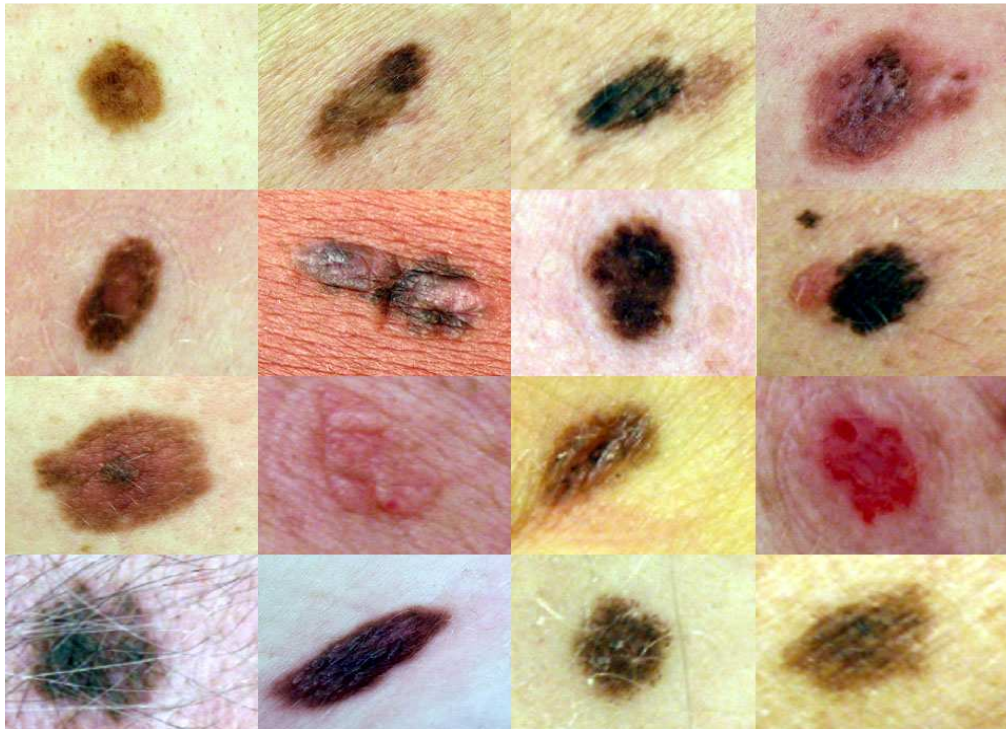


Figure 16 – Sixteen lesions overview pictures with permission by SciBase

Finding the melanoma without excising all of the lesions in Figure x is not an easy task and actually all lesions were considered by a dermatologist suspicious enough to warrant excision. The melanomas can be found in row 2 columns 2 and 3.

Depending on the physician's expertise, a dermatoscope will be utilized in the clinical diagnosis of a lesion. Basically, a modern dermatoscope consists of a magnifier (x10) and a polarized light source. The magnifier enhances the image of the lesion and the polarized light source helps to reduce the skin surface reflection. The skin surface reflection can be further reduced by applying a liquid medium (alcohol or some form of mineral oil) between the skin and the dermatoscope, enabling the higher detailed viewing of tissue structures underneath the stratum corneum

It has been shown that the use of a dermatoscope in clinical practice significantly improves diagnostic accuracy for melanoma, albeit as with everything a learning curve is involved. It takes time to learn how to differentiate the numerous structures that are revealed with help of a dermatoscope, since lesions start out looking more malignant before the new structures are accurately classified [63].

To help differentiate benign pigmented nevi and malignant melanoma various classification algorithms for dermatoscopy have been developed of which the most well known and applicable are ABCD-dermatoscopy [64], Menzies [65] and the 7-point

checklist [66]. These classifiers basically sum up the different features or assign weights to them prior to summing them up and applying fixed cut-offs for either excision recommendation, follow-up or leaving the lesion in the skin.

Interestingly, about 50% of the diagnosed melanomas are actually discovered by the patients themselves. A phrase one often comes across is: “A large proportion of old men come to the clinic after having been nagged by their spouses to check their atypical lesions, especially on their back. Often enough these turn out to be malignant.”

### **6.3.1 Clinical diagnosis**

Even though physicians feel fairly confident with making the distinction between non-suspicious and suspicious lesions using either only the naked eye together with patient history, or with the additional information obtained from dermatoscopy, their sensitivity in general has been shown to be far from 100% [67-70]. The accuracy of the clinical diagnosis of cutaneous melanoma with the unaided eye is only about 60% (sensitivity) [63], which improves to about 90% with the help of dermoscopy, but only when used by a trained/experienced user. These sensitivity values are however far from acceptable, why clinicians use a safety margin in their clinical diagnosis, and have an overall excision rate ~1:40. [67-71].

The consequences of the physician's low sensitivity for detecting a melanoma are at least twofold. Firstly, since early detection is vital for treatment outcome and survival a large number of benign lesions will be excised, thus creating a safety margin by reducing the number of missed melanoma. This is directly reflected in the biopsy ratios found in literature, ranging from ~80 lesions excised for every melanoma (1:80) to 1:~20 for a general practitioner, 1:30 to 1:8 for a general dermatologist, down to a ratio of 1:~3:4 for expert dermatologist specializing in melanoma detection [67-71]. Secondly, misdiagnosing melanoma is inevitable as early melanoma often show very few signs of malignancy and as direct consequence are going to be mistaken for a benign lesion, even by the most expert dermatologists. This is reflected in the fact that one of the most common causes for malpractice litigations against physicians is misdiagnosis of melanoma [72], which of course also adds to more benign lesions being excised. The need for additional tools in melanoma detection that can supply the physician with additional information about possible atypical lesions appears to be apparent.

## **6.4 HISTOPATHOLOGY DIAGNOSIS**

Once the physician has a suspicion for malignancy the lesion is excised (biopsied) and sent on to a histopathologist for evaluation and final diagnosis. The histopathological evaluation is done under microscope, where the histopathologist takes a large number of possible malignant patterns and indicators into consideration. In Figure 17, a Tis melanoma situated on the shoulder of a 48 year old male stained with hematoxylin and eosin is shown under 16.2x magnification.

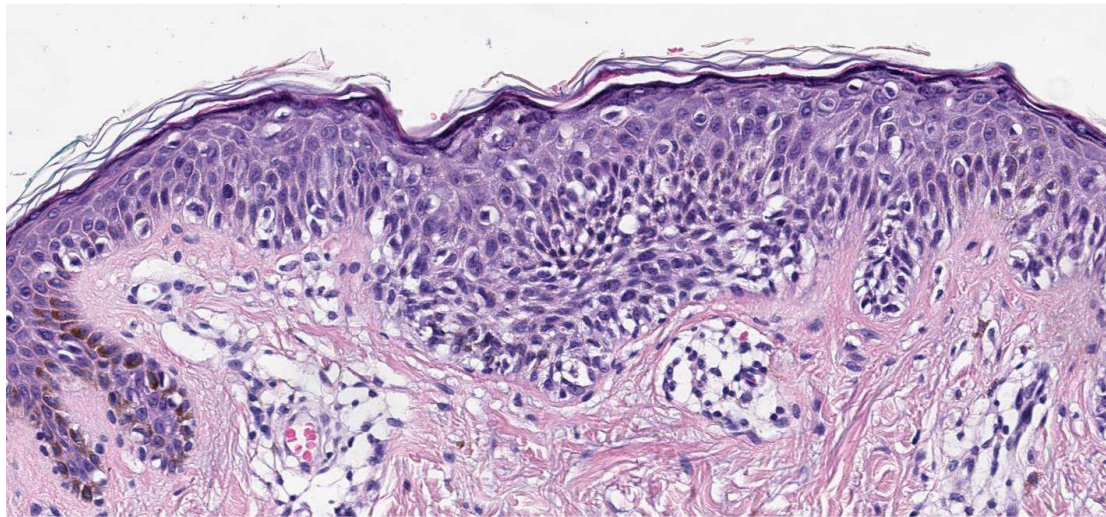


Figure 17 – Malignant melanoma, as seen by the histopathologist under the microscope.

Since the analysis is both visual and done by a human being it remains subjective and as a consequence not perfect, i.e. not 100%. A number of studies have shown a significant discordance between histopathologist in the diagnosis of melanoma [73-76]. Therefore a histopathology board, consisting of 3 histopathologist, reviewed each lesion independently of each other in Study I and II to ensure adequate accuracy in the reference/gold standard. The observed sensitivity of the local pathologist for melanoma in Study II was 86.1% (192/223) (80.9, 90.4) (observed sensitivity between 80.9 and 90.4 within a two-sided 95% Clopper-Pearson confidence interval), non-melanoma skin cancer 96.9% (95/98) (91.3, 99.4) and the observed specificity 92.6% (736/795) (90.5, 94.3). Evidently, histopathologists may misdiagnose malignant melanoma and other cancer, but it still is the best reference standard available and thus referred to as the gold/reference standard.

## 6.5 CLINICAL STUDY DESIGN

Clinical study design is essential to ensure that sufficient data is gathered, either to calibrate a classifier or to support the safety and efficacy endpoints.

Ensuring that the study conforms to the **I**nternational **C**onference of **H**armonization of **G**ood **C**linical **P**ractice (ICH-GCP) guidelines is essential, and even though one might think the adherence to this standard is given; experience has shown that frequent monitoring and education of how this guideline is to be adapted in the clinical setting is essential to ensure compliance.

Furthermore there are a couple of things to consider:

- Ensuring the correct cohort/population is studied, e.g. those lesions and patients which will be within the scope of the intended use of the device are to be studied. This is often referred to as intended use population.
- Correct proportion of lesions, i.e. both benign and lesions of varying degree of malignancy need to be studied. Having only the most benign and the most

malignant lesions present as input data will not enable estimation on the true accuracy of the device.

- Correct amount of lesions, based on reasonable assumptions on device accuracy, i.e. sensitivity and specificity, to ensure a sufficient statistical power of the study.
- Choosing the amount of sites, site location and considering both the referral population and the plausible inclusion rates into the study.
- Ensuring reasonable accuracy in the reference/gold standard.
- Adding a possibility to reference the outcome towards the clinical decision.
- Monitoring of the data and the sites. This point cannot be stressed enough. Poor data will remain poor data and interfere with the analysis of the data.
- Clear data management standard operating procedures.
- The ability to communicate clearly is essential. A substantial help can be to ensure that communication can be established in the native tongue.

## **6.6 DATA COLLECTION**

To give a brief overview of how intricate a clinical study design can look like, the pivotal trial for the SciBase III system is presented in Figure 18.

1. After obtaining the informed consent for each patient, eligible lesions fulfilling the inclusion/exclusion criteria and destined for excision/biopsy were categorized as having either low/mid/high risk of being malignant.
2. Thereafter, a photo and a dermatoscopy image were taken of the lesion and the lesion was subsequently measured with the SciBase system.
3. A second photo of the lesion post measurement was taken, and the lesion was surgically excised/biopsied and subjected to histopathological evaluation
4. The first analysis was performed by the local pathologist and a second analysis, the gold standard, was performed independently by a panel of three expert pathologists
5. In case of disagreement in the panel, the lesions were reviewed by a Consensus Board, consisting of an additional 2 histopathologists.
6. The photo and dermatoscopy images taken prior to SciBase measurement were evaluated by a Visual Classification Board for a uniform visual classification of all lesions according to e.g. ABCD criteria and 7-point checklist for dermatoscopy

All data was kept at an independent Contract Research Organisation (CRO) to ensure that the data remained blinded throughout the study.

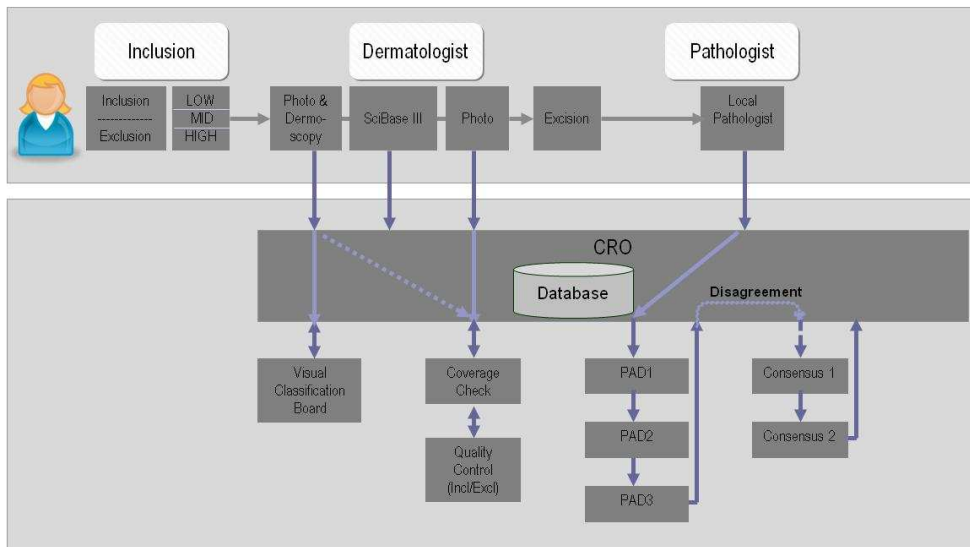


Figure 18 – Schematic overview of the study design for the pivotal trial of the SciBase III system.

## 6.7 DATA ANALYSIS OF ELECTRICAL IMPEDANCE MEASUREMENTS

The complexity in the analysis of bio-impedance spectra arise just due to the fact that it is complex valued and highly multivariate as it encompasses measurements conducted at multiple frequencies. For example the SciBase III impedance spectrometer measures 35 frequencies distributed between 1 kHz and 2.5 MHz at either 5 depth settings or 10 permutations settings, giving rise to 175 or 350 complex impedance values.

One important observation is that all the frequencies are highly cross-correlated to each other and can be given as both real (resistance) and imaginary (reactance) values or as magnitude and phase shift.

### 6.7.1 Principle component analysis (PCA)

Principle component analysis aims to reduce the dimensionality of the data whilst maintaining as much information or variance as possible. This is achieved by first finding the direction having the largest variance, first principal component, and thereafter finding subsequent directions, principal components, under the constraint that they are orthogonal to the previous principal components.

The application of PCA on a dataset in 3D is illustrated in Figure 19. Note that the observations are positioned on a plane in 3D, i.e. they can be described by a 2 principal components without any direct information loss.

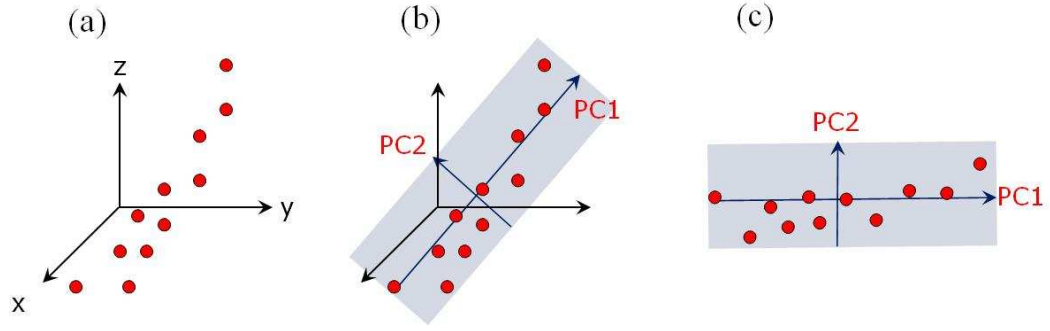


Figure 19 – (a) Observations in 3D. (b) Application of PCA to find the principal components. (c) Observations given in new Cartesian coordinates.

As this method aims to capture as much variance as possible in any given dataset it is of great importance to correctly scale the dataset prior to applying PCA, since otherwise essential information might be lost. Furthermore, outliers in the data need to either be excluded or treated with caution as they most likely will impact how the principal component space is formed.

For electrical impedance, where the frequencies are highly cross-correlated to each other this method is very effective to reduce data dimensionality without losing much information. Often a data matrix with electrical impedance data can be reduced to 3-5 dimensions encompassing approximately 95-97% of the variance found in the initial data. This is not a method optimized for categorizations, but can be extremely useful in the initial exploratory analysis.

The equation for the decomposition can be written as

$$\mathbf{X} = \mathbf{t}_1 \mathbf{p}'_1 + \mathbf{t}_2 \mathbf{p}'_2 + \dots + \mathbf{t}_a \mathbf{p}'_a + \mathbf{E}$$

$$\mathbf{X} = \sum_{a=1}^A \mathbf{t}_a \mathbf{p}'_a + \mathbf{E} = \mathbf{T} \mathbf{P}' + \mathbf{E}$$

where  $\mathbf{X}$  is the initial data matrix,  $\mathbf{t}_i$  is the  $i$ :th principal component score vector,  $\mathbf{p}_i$  is the  $i$ :th principal component vector,  $\mathbf{E}$  is the residual matrix (containing noise),  $\mathbf{T}$  is the score matrix, e.g.  $[\mathbf{t}_1 \mathbf{t}_2 \dots \mathbf{t}_A]$ , and  $\mathbf{P}$  the loading matrix, e.g.  $[\mathbf{p}_1 \mathbf{p}_2 \dots \mathbf{p}_A]$ .

From the decomposition formula above, one can deduce that the number of principal components is equal to the smallest dimension of  $\mathbf{X}$ . In case all principal components are used, the initial data matrix will only have been mapped into a new Cartesian coordinate system, albeit without any data or noise reduction. The variance captured by the principal components will be largest in the first and thereafter in descending order, i.e. less and less information will be pertained in the principal components. Therefore, there will be an optimal number of principal components that ought to be included in the reduced data matrix [77-79].

## 6.8 CLASSIFIERS

As with all classification tasks, the pre-processing task is vital and if it has not turned the data into something sensible, any classifier calibration will be “exciting”.

Furthermore, it is important that the reference standard for each observation is as accurate as it can possibly be, even though some noise has been shown to improve classification, a poor reference standard might introduce too much noise, making the calibration of any classifier impossible. Depending on the feature space, different classifiers might be more suitable than others.

### 6.8.1 k-nearest neighbors (k-NN)

The k-nearest neighbors is a very simple classification algorithm, which is based on the majority of the k nearest neighbors to the observations to be classified. In the case given in Figure 20, if k equals 1 the three unknown cases ■ will be classified as ●, ▲ and ▲ from left to right, respectively.

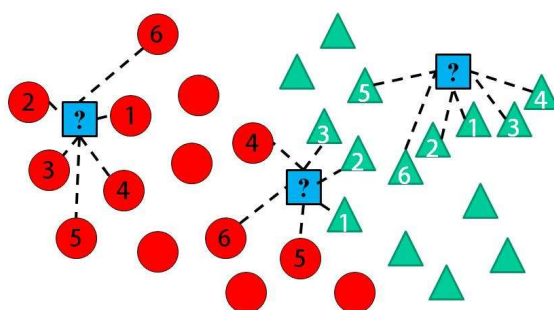


Figure 20 – Group A (●), Group B (▲) Group unclassified (■).

Note that if k equals 6, the middle unknown case will have equally many ●, ▲ and no decision can be made based on the nearest neighbors only. One way to resolve the deadlock could be to either sum the distances to each group respectively and assign it to the one “closest” to the given observation, or simply a larger or smaller k for these cases. By choosing an odd k, this situation can of course altogether be avoided.

The calculation of the distance to the nearest neighbors can be made in many different ways, for example using the Euclidean distance or the Manhattan distance.

### 6.8.2 Support vector machine (SVM)

For the case of a binary classification problem, a support vector machine constructs a hyperplane (generalization of a plane in a multidimensional space) with the best possible separation (margin) between the two groups to be classified in an often high-dimensional space. In Figure 21 a hyperplane is shown separating two groups with an optimal separation (margin) between the two groups.

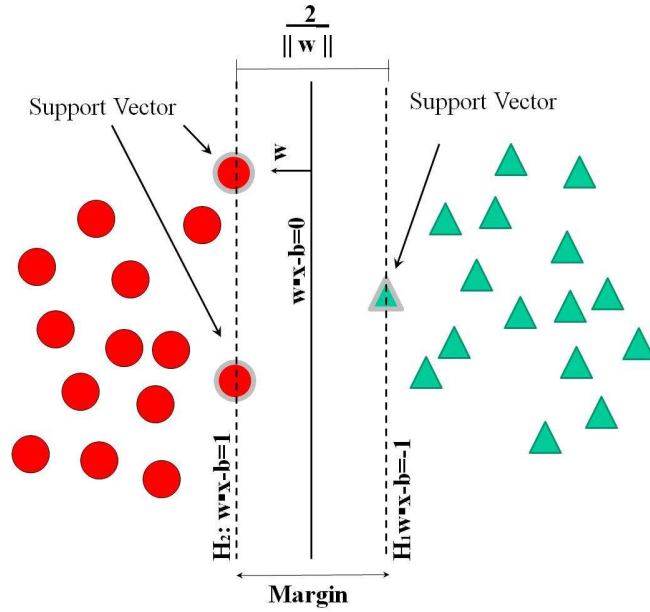


Figure 21 – The optimal hyperplane marked with a solid line between group A (●) and group B (▲) after support vector machine calibration. The observations on  $H_1$  and  $H_2$  are called the support vectors as they support the two sub-hyperplanes.

Any given plane (hyperplane) can be written as

$$\mathbf{w} \cdot \mathbf{x} - b = 0$$

where  $\mathbf{w}$  is the normal vector to the plane and any point  $\mathbf{x}$  that satisfies the equation will be situated thereon.

In the basic case where the groups are linearly separable, i.e. a line can be drawn between the groups without the groups overlapping, we want to try to maximize the margin between the two groups. The two hyperplanes  $H_1$  and  $H_2$  as depicted in Figure 21 can be described by the following two equations

$$\mathbf{w} \cdot \mathbf{x} - b = 1$$

$$\mathbf{w} \cdot \mathbf{x} - b = -1$$

Simple geometry gives us the distance between  $H_1$  and  $H_2$  to be  $\frac{2}{\|\mathbf{w}\|}$ , which is the margin that should be maximized. This is accomplished by minimizing the denominator, i.e.  $\|\mathbf{w}\|$ . Since we do not want any data points to fall within the margin during training, this leaves us with the following equations for the two different groups

$$\mathbf{w} \cdot \mathbf{x}_i - b \geq 1$$

$$\mathbf{w} \cdot \mathbf{x}_j - b \leq -1$$

where  $\mathbf{x}_i$  and  $\mathbf{x}_j$  are the data points for the first and second group, respectively. This can more conveniently be written as

$$y_i(\mathbf{w} \cdot \mathbf{x}_i - b) \geq 1$$

where  $y_i$  is either -1 for the first group and +1 for the second group or vice-versa and  $x_i$  are the specific observations coordinates.

The power of SVM is that even non-linearly separated groups (no plane can be drawn in the input space) can easily be solved by applying a kernel, which maps the input space into a higher dimensional feature space where the groups “suddenly” are separable by a hyperplane once more. In the case when no hyperplane can be found that separates the groups entirely, slack variables can be introduced to allow for softer hyperplane margins [80].

## 6.9 CLINICAL EFFICACY ENDPOINTS

### 6.9.1 Sensitivity and specificity

Before moving into the definition of sensitivity and specificity a word of caution is necessary to emphasize that even though these measures of accuracy can easily be calculated, they are not always easily interpreted. They must always be viewed in regards to the studied population and the accuracy of the used gold standard. Furthermore, they may under no circumstances be viewed separately, since there will almost always be a trade-off between the measures.

Sensitivity is a measure of the proportion of correctly classified positives (people with the disease under investigation). This, simply stated, is the percentage of people who are correctly identified as having the disease.

$$Sensitivity = \frac{\text{True Positives}}{\text{True Positives} + \text{False Negatives}}$$

Specificity on the other hand is a measure of the proportion of correctly classified negatives (people that do not have the disease under investigation). This, simply stated, is the percentage of people who are correctly identified as not having the disease.

$$Specificity = \frac{\text{True Negatives}}{\text{True Negatives} + \text{False Positives}}$$

Sensitivity and specificity are observed values in a study and should be referred to as the observed sensitivity and specificity, except in the case where the confidence bound of the observations is very small.

In melanoma diagnosis, missing a melanoma can have dire consequences and therefore it is essential to have as high sensitivity as possible without sacrificing too much specificity.

### 6.9.2 ROC – Receiver operating curve

It is often of interest to evaluate the overall discriminate power of a binary classifier, e.g. not only at a fixed cut-off between what is to be considered benign (0) and malignant (1). This can be accomplished by varying the discrimination threshold from

the minimum to maximum value of the classifier outcome and for each step calculating the sensitivity and specificity as illustrated in Figure 22.

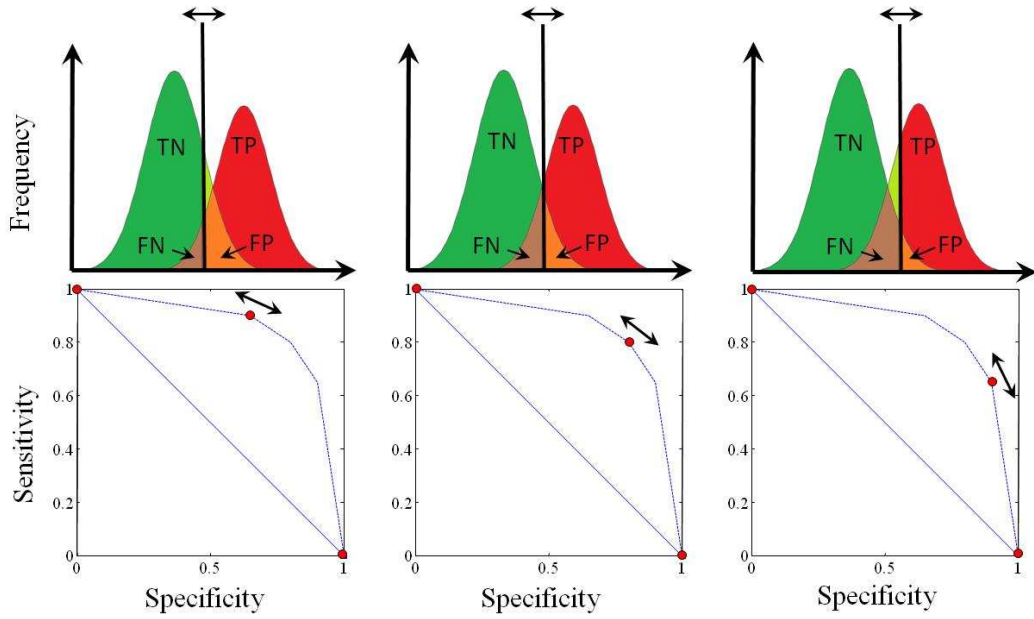


Figure 22 – (Upper row) Moving threshold (Lower Row) calculated sensitivity and specificity at the given discriminative threshold.

The calculated values for sensitivity and specificity, as shown in Figure 22, are used to obtain a receiver operating curve (ROC). Note that at the starting point the sensitivity is 0% and increases to 100% whilst the specificity decreases from 100% to 0%.

The overall discriminate power of a binary classifier equals the area under the receiver operating curve (AUC). This value will span from 0 to 1 or 0% to 100%, where an area of 50% is equivalent to a random classification or flipping a coin, and 100% to an ideal classifier, where all cases are correctly classified. In melanoma applications a practical interpretation of the AUC is that  $\geq 90\%$  is considered excellent,  $\geq 80\%$  good,  $\geq 70\%$  OK,  $\geq 60\%$  poor and  $\geq 50\%$  worthless [81].

Since the area under the curve (AUC) is an estimate of the overall performance of a binary classifier the standard error of the estimation can be calculated. As ROC analysis is non-parametric, i.e. the data does not adhere to a normal distribution, the confidence intervals can be conservatively calculated as follows [82]:

$$\sigma_{AUC}^2 = \frac{AUC(1 - AUC) + (n^+ - 1)(q_1 - AUC^2) + (n^- - 1)(q_2 - AUC^2)}{n^+ n^-}$$

where  $n^+$  and  $n^-$  are number of positive and negative events respectively, and  $q_1$  and  $q_2$  are given as

$$q_1 = \frac{AUC}{2 - AUC}$$

$$q_2 = \frac{2 \times AUC^2}{1 + AUC}$$

Keep in mind that this is one measure of overall discriminate performance, which has shown itself to be highly applicable in many medical applications [63, 83-84], although there might be other constraints that need to be considered, prior to choosing a binary classifier for a given classification task, such as the point of performance, e.g. sensitivity above 95% being a necessity.

### **6.9.3 Safety**

A safety assessment aims to quantify how safe the device or treatment is. To gather the information necessary to evaluate the safety of a device or treatment all unfavorable and unintended reactions to a device or medical treatment (Adverse Events) that occur during a pivotal study need to be documented (once the product is released onto the market, the adverse events still need to be monitored to ensure the safety of the treatment or device). Depending on the severity of the adverse event, they are classified as either serious adverse events (SAE) or just adverse events (AE). Serious adverse events, may they be device or treatment related or not, must be reported to the regulatory authorities within 48 hours. To give an example, diarrhea for 2 days following the surgical excision of a mole can be considered an adverse event and is generally resolved without the need for hospitalization. On the other hand, if the patient falls and breaks a leg during the course of a study and is hospitalized this is to be considered a serious adverse event. To help understand why this is so, it might be that the treatment or the application of a medical device has given the patient impaired balance or nausea which then resulted in the fall.

At the end of a study the occurred adverse events are summed up and a safety assessment of the treatment or device can be undertaken and fed into a risk/benefit analysis.

## 7 MATHEMATICAL MODELING OF SKIN

### 7.1 INTRODUCTION

Implementing a generic mathematical model of the skin can (i) aid in the design and operation of the electrodes, (ii) increase the probability of extracting the most relevant signals and (iii) also be implemented to evaluate the feasibility of an impedance study. A generic model, however, that aims to capture all the physiochemical phenomena, tissue types and structures inside the various layers of the skin—hair follicles, pores [85], sweat ducts [85], pH gradients [86], diurnal variations [87] as well as a multitude of other factors—can easily lose tractability; therefore, simplifications in the mathematical formulation are usually invoked [19-20, 22-24, 29, 88].

### 7.2 SKIN COMPOSITION

We assume that the skin can be modeled as a three-layer entity, comprising Stratum Corneum (SC), Viable skin (VS), and Adipose tissue (AT), where the Epidermis and Dermis are incorporated into the viable skin, and subcutis into the adipose tissue (see Figure 23c).

The skin thickness, which is an important parameter in the mathematical model for skin impedance, naturally varies due to a large number of biological and environmental factors –age, time of the day, race, temperature, humidity, health condition, and so forth. Furthermore, variations in measured skin thickness can arise due to the type of measurement technique that is employed; other factors include measurements where the sample size is too small to allow for statistical analysis and/or where the exact location of measurement is not specified. In light of the large number of factors and errors, a mean thickness and standard deviation were calculated by summing up the skin thicknesses for a female cohort from several studies, which include a variety of techniques and weighing them equally: confocal Raman spectrometer [89-91], optical coherence tomography [91], reflectance confocal microscopy [92], ultrasound imaging [93-95], biopsy [96] and transepidermal water loss (TEWL) in combination with Stratum corneum stripping [97-100]. The viable skin was calculated by adding the viable epidermis thickness to the dermal thickness comprising both papillary and reticular dermis (see Figure 23c). The stratum corneum thickness  $h_{sc}$  was found to be  $14 \pm 3 \mu\text{m}$  and the viable skin  $h_{VS}$   $1.2 \pm 0.2 \text{ mm}$  at the volar forearm. The subcutaneous fat thickness was set to  $1.2 \pm 0.2 \text{ mm}$

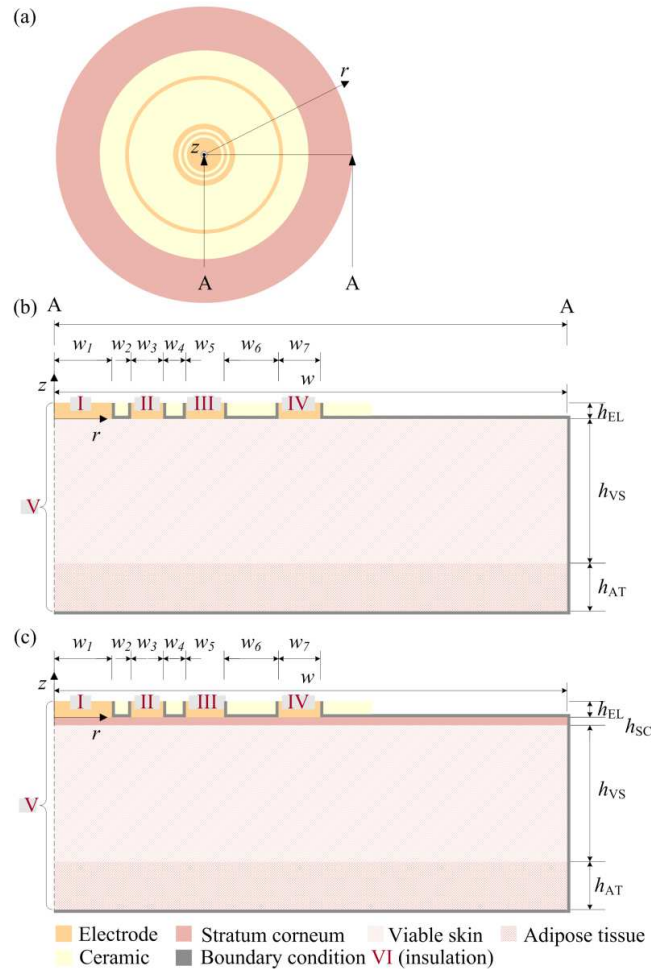


Figure 23 – Schematic overview of the circular non-invasive electrode applied on (a) skin, (b) viable skin and adipose tissue, and (c) stratum corneum, viable skin and adipose tissue. Length scales are shown for the different skin layers and electrodes of the circular probe; boundary conditions for the mathematical model are given by roman numerals for easy identification.

### 7.3 ELECTRICAL IMPEDANCE ELECTRODE

In studies I, II and III the non-invasive, circular probe comprises four electrodes as illustrated in Figure 23: two voltage injection electrodes (III and IV), one current detector (I) and one guard electrode (II) to decrease the impact of surface leakage currents. With this design, two-point measurements can be carried out. The dimensions of the electrode can be found in either Study 3, 4 and 5.

The electrode can be adapted to any shape and size, but the electrode given here was chosen since the experimental measurements were carried out utilizing that particular electrode.

### 7.4 MATHEMATICAL MODEL

In this part the governing equations for a time-harmonic quasi-static electric current are derived. Similar models have been introduced and discussed by Bedard et al.[101] and Miller et al.[102]

### 7.4.1 Governing equations in the transient domain

For the most general case, the Maxwell equations can be written in differential form as

$$\nabla \times \mathbf{H} = \mathbf{J} + \frac{\partial \mathbf{D}}{\partial t}, \quad (1)$$

$$\nabla \times \mathbf{E} = -\frac{\partial \mathbf{B}}{\partial t}, \quad (2)$$

$$\nabla \cdot \mathbf{D} = \rho, \quad (3)$$

$$\nabla \cdot \mathbf{B} = 0; \quad (4)$$

here,  $\mathbf{H}$  is the magnetic field intensity,  $\mathbf{J}$  is the current density,  $\mathbf{D}$  is the electric displacement,  $\mathbf{E}$  is the electric field intensity,  $\mathbf{B}$  is the magnetic flux density,  $\rho$  is the electric charge density, and  $t$  denotes time. In addition, one generally defines the equation of conservation of charge as

$$\frac{\partial \rho}{\partial t} + \nabla \cdot \mathbf{J} = 0. \quad (5)$$

We proceed by treating the various layers of the skin as linear isotropic conductors, for which we can write the electric displacement,  $\mathbf{D}$ , the magnetic flux density,  $\mathbf{B}$ , the electric field intensity,  $\mathbf{E}$ , and current density,  $\mathbf{J}$ , as

$$\mathbf{D} = \epsilon_0 \epsilon_r \mathbf{E}, \quad (6)$$

$$\mathbf{B} = \mu_0 \mu_r \mathbf{H}, \quad (7)$$

$$\mathbf{J} = \sigma \mathbf{E}, \quad (8)$$

$$\mathbf{E} = -\nabla \phi - \frac{\partial \mathbf{A}}{\partial t}, \quad (9)$$

where  $\epsilon_r$  and  $\mu_r$  are the relative permittivity and relative permeability of the material, respectively,  $\epsilon_0$  and  $\mu_0$  are the permittivity and permeability of vacuum, respectively,  $\sigma$  is the electric conductivity,  $\phi$  is the electric potential and  $\mathbf{A}$  is the vector magnetic potential.

To simplify the Maxwell equations further, we exploit the fact that dimensions of the human skin and probe are small compared to the wavelengths, which in turn implies that the impedance measurements can be considered quasi-static, i.e.  $\partial \mathbf{D} / \partial t = 0$ .

Furthermore, the electromagnetic penetration depth is much larger than the domain under consideration, whence the electric and magnetic fields decouple, i.e.

$$\nabla \times \mathbf{E} = 0 \quad (10)$$

such that there are no induced currents. This decoupling simplifies the constitutive relation for the electric field, equation (9), to

$$\mathbf{E} = -\nabla\phi. \quad (11)$$

We proceed by substituting the constitutive relations for the electric field, equation (11), electric displacement, equation (6), and current density, equation. (8), into Eq. (5), which yields

$$\frac{\partial}{\partial t}(\nabla \cdot (\epsilon_0 \epsilon_r \nabla \phi)) + \nabla \cdot (\sigma \nabla \phi) = 0. \quad (12)$$

#### 7.4.2 Governing equations in the frequency domain

Finally, we simplify Eq. (12) further by noting that the impedance probe employs a time-harmonic electric field, which in turn allows for a transformation to the frequency domain by introducing a phasor, defined as

$$\mathbf{E}(\mathbf{r}, t) = \hat{\mathbf{E}}(r) \cos(\omega t + \psi) = \text{Re}(\hat{\mathbf{E}}(\mathbf{r}) e^{j\psi} e^{j\omega t}) = \text{Re}(\tilde{\mathbf{E}}(\mathbf{r}) e^{j\omega t}), \quad (13)$$

where  $\tilde{\mathbf{E}}(\mathbf{r})$  is a phasor that is a function of space but not time,  $\omega$  is the angular frequency,  $\psi$  is the phase of the signal, and  $j$  is the imaginary unit. We further require a time derivative in Eq. (12), which can be determined from

$$\frac{\partial}{\partial t} \mathbf{E}(\mathbf{r}, t) = \frac{\partial}{\partial t} \text{Re}(\tilde{\mathbf{E}}(\mathbf{r}) e^{j\omega t}) = \text{Re}(j\omega \tilde{\mathbf{E}}(\mathbf{r}) e^{j\omega t}). \quad (14)$$

Substituting the phasor and its time derivative - the time derivative  $\partial/\partial t$  can now be replaced with  $j\omega$  into Eq. (12) yields an elliptic partial differential equation (**N.B.:** we drop the tilde for the phasor):

$$\nabla \cdot ((\sigma + j\omega \epsilon_0 \epsilon_r) \nabla \phi) = 0. \quad (15)$$

#### 7.4.3 Boundary conditions

We solve this differential equation throughout the computation domain subject to the following boundary conditions (boundaries denoted by roman numerals in Figure 23):

- At the sense (I) electrode and guard electrode (II), we specify a ground potential:

$$\phi = 0 \quad (16)$$

- At the injection electrodes (III, IV), we prescribe a variable potential:

$$\phi = \alpha V_0 \text{ (III)} \quad (17)$$

$$\phi = V_0 \text{ (IV)} \quad (18)$$

where  $\alpha$  varies from 0.1 to 1 depending on the depth setting, as described in Section 6.2.3

- At the insulated boundaries (VI), we set no-flux conditions:

$$\mathbf{n} \cdot \mathbf{J} = 0 \quad (19)$$

where  $\mathbf{n}$  is a vector normal to the boundary. The insulated boundaries (VI) either represent (i) the interface between skin and air or (ii) the interface between the computational domain and adjacent skin, which is sufficiently far away from the probe that the currents there are negligible.

In case the electrode design changes to only encompass one injection electrode and one sense electrode the boundary equations x and y can be dropped.

#### **7.4.4 Constitutive relations**

The electric resistivity and relative permittivity of stratum corneum and viable skin in the frequency range 1-10<sup>3</sup> kHz are taken from Birgersson et al [31] and the subcutaneous fat from Gabrielle et al. [103].

### **7.5 ANALYTICAL SOLUTION**

It is well known that the stratum corneum heavily dominates the electrical impedance at low frequencies around 1 kHz [28-29], which suggests that the potential drop over the viable skin is negligible and the complete potential drop, occurs over the stratum corneum. This can be shown to be the case by conducting a scaling analysis as was done by Birgersson et al. [32]. Furthermore, by assuming that the currents pass orthogonal to the electrodes when entering through the stratum corneum the full set of equations given in section 7.4 could be reduced to a set of algebraic equations. Solving these equations resulted in closed-form analytical expressions for electrical impedance, magnitude, phase, electrical properties as well as the thickness of stratum corneum, which can be found in Paper V.

### **7.6 MODEL LIMITATIONS**

As with all models there are limitations to their usage and it is vital that they are only applied within their region of validity.

## 8 RESULTS AND SHORT DISCUSSION

### 8.1 STUDY I

In Study I, electrical impedance spectra were measured in a multi-centre study at 12 clinics around Europe. Data from 285 histologically analyzed lesions were used to calibrate an algorithm to sort out lesions for automatic detection of melanoma. A separate cohort, collected consequently after the training set, consisted of 210 blinded lesions (148 various benign lesions and 62 malignant melanomas with a median Breslow thickness of 0.7mm) from 183 patients which was used to estimate the accuracy of the technique.

A total of five different classifier candidates were trained, four of these candidates were trained using only the EIS data for each of the numerical techniques partial least squares discriminant analysis (PLS-DA), support vector machine (SVM), artificial neural network (ANN) and k-nearest neighbours (kNN) techniques and a fifth classifier using PLS with only the clinical report form details gathered by the clinicians in the study, i.e. subject age, lesion size and area, ABCD and ulceration criteria representing clinically visible ulceration, true or false. The majority decision of the classifiers was used as outcome, since it showed a better overall performance in the training cohort than each individual classifier separately. The majority decision approach is rather simplistic, there are other alternatives to combine multiple classifiers including weighting of individual classifiers; however, this would require more data available in the training set. Furthermore, the influence of melanoma thickness and histopathology inter-observer reproducibility on the classifier outcome was analyzed using non-parametric Mann–Whitney U test.

The observed EIS sensitivity to malignant melanoma was 95% (59/62) with an observed specificity 49% (72/148). Classifier outcomes categorized according to histopathology diagnosis, Breslow thickness and naked eye ABCD criteria are listed in Table 5. Area under the ROC curve of the blind test set was 85% and the observed sensitivity for each specific classifier aNN, kNN, PLS-DA, SVM and PLS-DA trained with demographic data only were 97%, 90%, 95%, 97% and 90% respectively, and the observed specificity 39%, 59%, 46%, 51% and 51% respectively. Additionally, the results indicated that the observed sensitivity is correlated with the thickness of the melanomas, with a significant statistical difference between thin (Tis-T1) and thick malignant (T2-T4) melanomas. An initial comparison of the results with the thorough meta-analysis conducted by Kittler et al. [63] indicates that the present EIS technique is superior to the naked eye and to dermatoscopy by non-experts, but inferior to dermatoscopy by experts, even though a word of caution should be raised due to possible bias.

Table 5 Differentiated outcome and accuracy of the blinded test set. The melanomas are differentiated according to Breslow thickness, the dysplastic nevi according to histopathologic degree of atypia, and the benign nevi according to the number of ABCD criteria fulfilled by the lesions. The “other benign lesions” class includes five false positive seborrheic keratoses, one false positive fibrous histiocytoma, and one true negative undefined benign lesion. Not applicable entities are marked NA.

	TP	FN	TN	FP	EIS Sensitivity	EIS Specificity
<b>Malignant melanoma (total)</b>	<b>59</b>	<b>3</b>	<b>NA</b>	<b>NA</b>	<b>95%</b>	<b>NA</b>
<i>In situ melanoma</i>	10	0	-	-	100%	-
<i>≤ 1.0 mm Breslow thickness</i>	25	3	-	-	89%	-
<i>1.01 to 2.0 mm Breslow thickness</i>	10	0	-	-	100%	-
<i>2.01 to 4.0 mm Breslow thickness</i>	13	0	-	-	100%	-
<i>&gt; 4.0 mm Breslow thickness</i>	1	0	-	-	100%	-
<b>Dysplastic nevi (total)</b>	<b>NA</b>	<b>NA</b>	<b>48</b>	<b>48</b>	<b>NA</b>	<b>50%</b>
<i>Structural disorder only</i>	-	-	5	1	-	83%
<i>Mild to moderate dysplasia</i>	-	-	22	22	-	50%
<i>Severe dysplasia</i>	-	-	4	9	-	31%
<i>Undefined degree of dysplasia</i>	-	-	17	16	-	52%
<b>Benign nevi (total)</b>	<b>NA</b>	<b>NA</b>	<b>23</b>	<b>22</b>	<b>NA</b>	<b>51%</b>
<i>1 of 4 possible ABCD</i>	-	-	4	1	-	80%
<i>2 of 4 possible ABCD</i>	-	-	10	3	-	77%
<i>3 of 4 possible ABCD</i>	-	-	6	7	-	46%
<i>4 of 4 possible ABCD</i>	-	-	3	11	-	21%
<b>Other benign lesions (total)</b>	<b>NA</b>	<b>NA</b>	<b>1</b>	<b>6</b>	<b>NA</b>	<b>14%</b>
<b>TOTAL</b>	<b>59</b>	<b>3</b>	<b>72</b>	<b>76</b>	<b>95%</b>	<b>49%</b>

During the course of the study a number of desirable technical and study design improvements were identified. Such improvements involve re-designing the electrode array from a three bar electrode with dynamic depth selection to a five bar electrode with 10 specific selectable volume settings to enhance the accuracy for thin and heterogeneous malignant melanomas by increasing the current density and electric sensitivity field underneath the electrode. The probe required redesign to ensure that a fixed pressure is applied to the skin during the measurements to reduce operator dependency and thus improve the reproducibility of the technique. Additional improvements involve increasing the applied voltage from 50 to 250 mV to minimize the impact of external noise on the measurements. Furthermore, the clinical protocol should be adjusted to include the full range of lesions that are presented both in a specialist setting as well as in a GP setting and include the clinical diagnosis and categorization of dermatoscopic features of all included lesions.

## 8.2 STUDY II

In Study II, a total of 1300 lesions from 1134 subjects were collected in a multicentre, prospective, nonrandomized clinical trial at 19 clinics around Europe with the objective to calibrate a classifier with a sensitivity of at least 98% and a specificity approximately 20 percentage points higher than the diagnostic accuracy of dermatologist on suspicious lesions. All lesions were to be excised and subsequently evaluated independently by a panel of three pathologists. From the data two classification algorithms were trained and verified.

In Study I, five different classifier candidates were calibrated and the classifier outcome was based on the majority decision of those. However, since the best performance was established with a support vector machine, in line with general consensus in the field of machine learning of dichotomous classification tasks [80], two support vector machine classifiers were trained with different training cohorts using only EIS data obtained in Study II.

For the first classification algorithm, approximately 40% of the data was used for training and 60% for testing. The observed sensitivity for melanoma was 98.1% (101/103) (93.2, 99.8) (observed sensitivity between 93.2 and 99.8 within a two-sided 95% Clopper-Pearson confidence interval), non-melanoma skin cancer 100% (25/25) (86.3, 100) and dysplastic nevi with severe atypia 86.2% (32/38) (68.7, 94.0). The observed specificity for dysplastic nevi with mild to moderate atypia was 20.5% (38/185) (15.0, 27.1), benign melanocytic nevi and variants 42.2% (27/64) (29.9, 55.2), seborrheic keratoses 0% (0/22) (0, 15.4) and other lesions 11.1% (1/9) (0.28, 48.2). The overall specificity was 23.6% (66/280) (18.7, 29.0).

For the second classification algorithm, approximately 55% of the data was used for training and evaluated on the whole dataset, i.e. 45% of the data was not used in the training of the classifier. All lesions included in the training and verification had a valid histopathology, electrical impedance reading, fulfilling the inclusion and none of the exclusion criteria. The observed sensitivity for melanoma was 99.4% (161/162) (96.9, 99.98), non-melanoma skin cancer 98.0% (49/50) (89.4, 99.95) and dysplastic nevi with severe atypia 93.8% (60/64) (84.8, 98.3). One microcystic adnexal carcinoma was included in the study and was correctly classified as positive. The observed specificity for dysplastic nevi with mild to moderate atypia was 23.9% (77/322) (19.4, 29.0), benign melanocytic nevi and variants 35.5% (38/107) (26.5, 45.4), seborrheic keratoses 0% (0/28) (0, 12.3) and other lesions 5.9% (1/17) (0.2, 28.7). The overall specificity was 24.5% (116/474) (20.7, 28.6).

The observed sensitivity of the local pathologist for melanoma was 86.1% (192/223) (80.9, 90.4), non-melanoma skin cancer 96.9% (95/98) (91.3, 99.4) and the observed specificity 92.6% (736/795) (90.5, 94.3). The observed sensitivity of the dermatologist, for the eligible lesions, was 100% (162/162) (97.8, 100) and the specificity was 8.4% (40/474) (6.1, 11.3). However, it is important to note that the majority of the lesions

included in the study were preselected for excision with a suspicion for melanoma, i.e. per trial design a clinical sensitivity of 100% and specificity of 0%

The observed sensitivity of the device clearly met the target of at least 98% sensitivity. However, it fell somewhat short on the 20 percentage points higher specificity than clinical diagnosis of dermatologists, i.e. given 8.4% clinical specificity should have resulted in device specificity of approximately 28.4%. The reason is primarily twofold: First, the participating dermatologists were highly experienced in diagnosing cutaneous tumors with the naked-eye and by dermatoscopy, and as such their diagnostic accuracy might have been higher than that of the average dermatologist [63, 104-107]. Secondly, the majority of the lesions included in this study had been suspicious for melanoma and were destined for excision, which is why the clinical sensitivity and specificity, by study design, was 100% and 0% respectively. However, the true clinical specificity in this trial could be considered to fall somewhere between 0% and 8.4%, as a few lesions with a low probability for melanoma had been included.

### 8.3 STUDY III

In this study, a mathematical model of the skin, see Section 7, is implemented with the electrical properties for the stratum corneum and viable skin from Yamamoto et al. [27] and for subcutaneous fat from Gabriel et al. [18] to assess the model's ability to capture the overall impedic nature of the skin. Within the framework of this model, the impact of the thickness of the stratum corneum, viable skin and subcutaneous fat on electrical impedance measurements is analyzed.

After solving the mathematical model and comparing it to the experimental findings (soaking time 1 min; sodium chloride concentration of 0.9%), the predicted response deviated from the measured counterpart on the order of one magnitude. Part of the reason for the deviation was deduced to be due to the assumption made by Yamamoto et al. of a stratum corneum thickness of 40  $\mu\text{m}$  on the volar forearm, whilst a literature review found the stratum corneum thickness to be around 14  $\mu\text{m}$ . Since there is a linear dependency (resistivity) and inverse linear dependency (permittivity) on the mean electrical properties, the electrical resistivity and relative permittivity throughout the whole frequency domain were corrected with the ratio 40/14 and 14/40, respectively, as given in Figure 24.

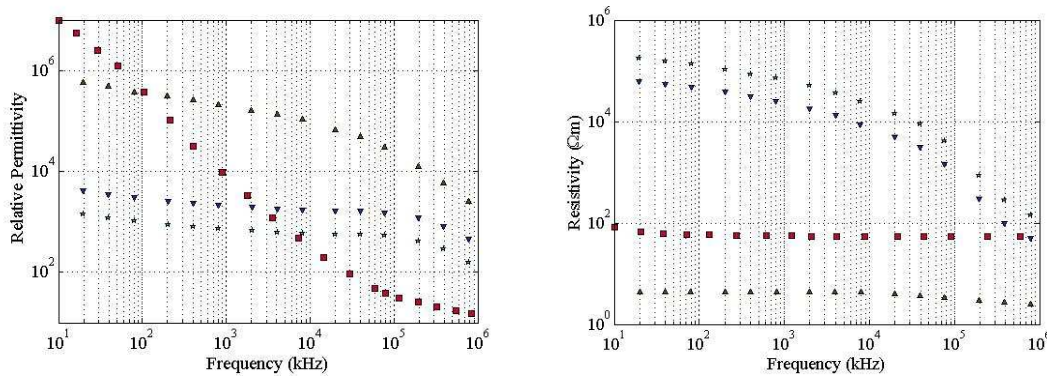


Figure 24 – (a) Average resistivities of (▼) stratum corneum, (★) adjusted stratum corneum, (▲) viable skin, (■) adipose tissue; (b) average relative permittivity of (▼) stratum corneum, (★) adjusted stratum corneum, (▲) viable skin, and (■) adipose tissue.

The results showed that the adjustments of the electrical properties of the stratum corneum decreased the difference between the magnitudes in the low and mid frequencies as well as the differences in phase shift at all frequencies. There was also an apparent shift in the slope change that now occurred around 50 kHz. Calculating the Cole–Cole alpha value for the adjusted model now yielded  $8.2 \pm 0.5^\circ$ , which is closer to the experimental alpha value. However, there still remained a difference between the mathematical model and the experimental counterpart.

Since Yamamoto et al. employed a Beckman electrode paste with an 18% sodium chloride concentration and let the skin soak for 30 min prior to measurements to estimate the average resistivity,  $\bar{\rho}_{sc}$ , and average relative permittivity,  $\bar{\epsilon}_{sc}$ , the deviation between model predictions and the impedance measurements found can most likely be explained by the moisturization period and the sodium chloride concentration. In view

of these two factors, the change in electrical impedance due to moisturization and sodium chloride concentration on a cohort of ten females were investigated. The results clearly showed that the solution with an 18% sodium chloride concentration significantly alters the electrical properties of the skin over time, whilst the skin moisturized with a physiological saline solution remains stable between roughly 1 and 10 minutes and undergoes a minor change thereafter.

Returning to the mathematical model and comparing it to the experimental impedance measurements after applying a moisturizer with 18% sodium chloride for 30 min, a better agreement between the experimental data and model predictions was found (see Figure 25); the magnitude and phase of the model are now within the  $\pm 1.96$  standard deviation of the experimental data. In the high frequency range, the magnitude for the adjusted model overshoots the experimental data.

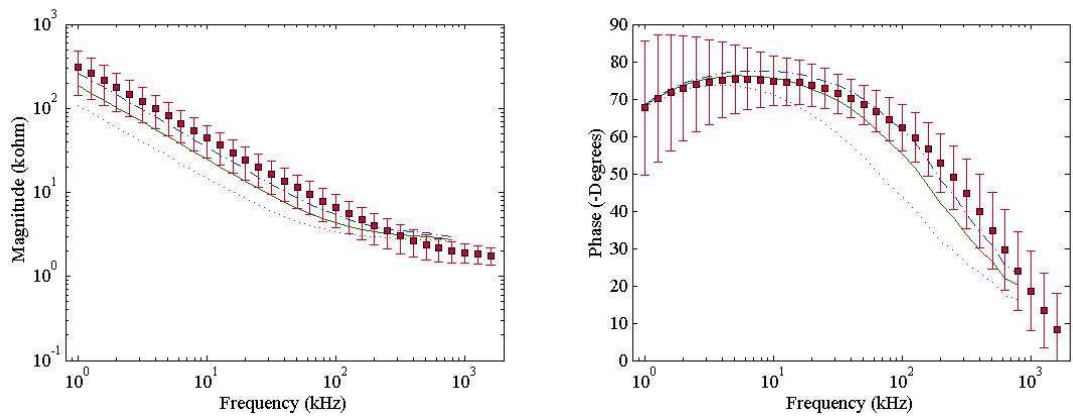


Figure 25 – (a) Magnitude of (■) the experimental data (18% sodium concentration) with errorbars representing  $\pm 1.96$  standard deviations, and model predictions based on the adjusted dielectrical properties of the SC derived from Yamamoto et al (1976) with (...) 8  $\mu\text{m}$ , (—) 14  $\mu\text{m}$  SC and (- - -) 20  $\mu\text{m}$  SC with a 1.2 mm thick VS. (b) Corresponding measured and predicted phase.

A mathematical model of the skin considering conservation of charge has been derived and experimentally validated. The findings led to an adjustment of the average resistivity and relative permittivity of the stratum corneum derived earlier by Yamamoto and Yamamoto (1976). By adjusting the dielectrical properties, we have arrived at a good agreement between the model predictions and experimental findings after application of an 18% sodium chloride solution for 30 min; however, when physiological saline solution is employed as a moisturizer, the model predictions are less accurate. Hence further improvements should be made to determine more accurate dielectrical properties of the stratum corneum and the underlying viable skin.

## 8.4 STUDY IV

In Study IV, a methodology to determine dielectrical properties of human skin was presented and analyzed. The therein proposed methodology rests on four pillars as illustrated in the flowchart in Figure 26: experimental measurements, optimization, automated code generation, and a mathematical model.

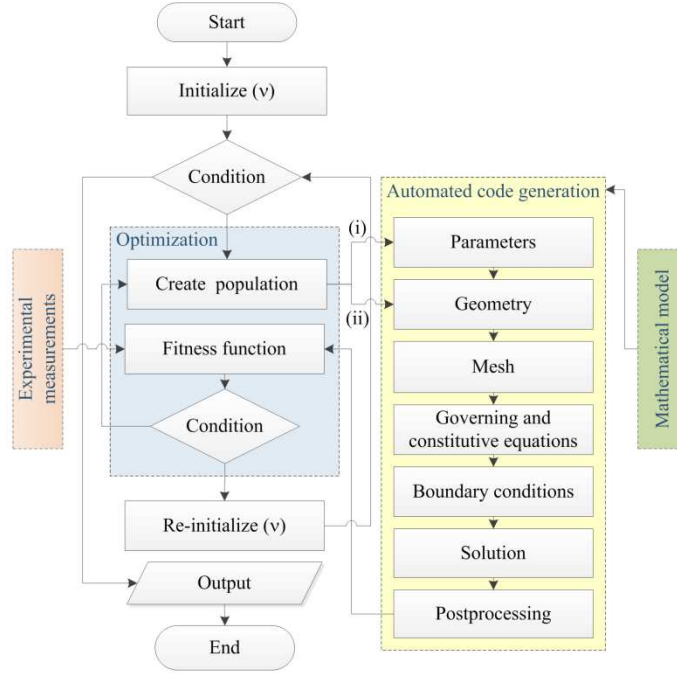


Figure 26 – Flowchart of the methodology — experimental measurements, optimization, automated code generation, and mathematical modeling — for extracting the electrical properties of human skin.

In essence, an optimization algorithm receives the electrical impedance from the experimental measurements,  $Z_{exp}$ , of an individual and provides estimates for the electrical parameters that are to be determined to the automated code generator; the latter, in turn, returns  $Z_{mod}$  to the optimization algorithm, which iterates until the fitness function  $f$ , given in Equation (20), has reached a certain tolerance.

$$f(Z_{mod}, Z_{exp}) = \frac{|Re(Z_{mod}) - Re(Z_{exp})| + |Im(Z_{mod}) - Im(Z_{exp})|}{|Re(Z_{mod})| + |Im(Z_{exp})|} \quad (20)$$

An outer for-loop then works through the measured frequency domain from 1 to  $10^3$  kHz for each individual.

First, this methodology was applied with the electrical impedance measurements obtained after stratum corneum strippings in order to decouple the electrical properties of the viable skin and the stratum corneum. The average electrical properties of the viable skin were calculated with the geometry illustrated in Figure 23b by setting the thickness of the viable skin,  $h_{VS}$ , and subcutaneous fat,  $h_{AT}$ , to the mean population thickness of 1.2 mm respectively. Once the functional forms for the average

permittivity and resistivity of the viable skin were secured, we proceeded with the measurements of intact skin. The average electrical properties of the stratum corneum were calculated with the geometry illustrated in Figure 23c by setting the thickness of the viable skin,  $h_{VS}$ , subcutaneous fat,  $h_{AT}$ , and stratum corneum,  $h_{SC}$ , to the mean population thicknesses of 1.2 mm, 1.2 mm and 14  $\mu$ m, respectively.

For the estimation of the electrical properties of viable skin, the electrical impedance measurement from 26 healthy volunteers, having had the 80 stratum corneum strippings performed on the volar forearm with Scotch® Magic™ Cellulose Tape, was used. In the estimation of the electrical properties of the stratum corneum, measurements from the baseline study on intact skin, encompassing a total of 120 volunteers, was utilized in conjunction with the electrical properties obtained for the viable skin.

The median electrical properties of the viable skin and stratum corneum in the frequency range 1-10<sup>3</sup> kHz, obtained from the first and second study respectively, can conveniently be written as exponential functions in log space:

$$\rho^{sc}(\Omega) = 10^{0.011516\Omega^5 - 0.25509\Omega^4 + 2.2537\Omega^3 - 9.9955\Omega^2 + 21.404\Omega - 11.803}, \quad (21)$$

$$\varepsilon_r^{sc}(\Omega) = 10^{-0.011319\Omega^5 + 0.23953\Omega^4 - 2.0255\Omega^3 - 8.5278\Omega^2 - 17.961\Omega + 17.570}, \quad (22)$$

$$\rho^{sc}(\Omega) = 10^{-0.015178\Omega^5 + 0.23953\Omega^4 - 2.0255\Omega^3 + 8.5278\Omega^2 - 17.961\Omega + 23.688}, \quad (23)$$

$$\varepsilon_r^{sc}(\Omega) = 10^{-0.044465\Omega^5 + 0.92429\Omega^4 - 7.7649\Omega^3 + 32.847\Omega^2 - 70.466\Omega + 67.610}. \quad (24)$$

These functions are illustrated in Figure 27 with the population variability as 25/50/75 percentiles and upper and lower ranges based on the 1.5 interquartile range rule (equivalent to the boxplot for discrete data; the 50 percentile corresponds to the median).

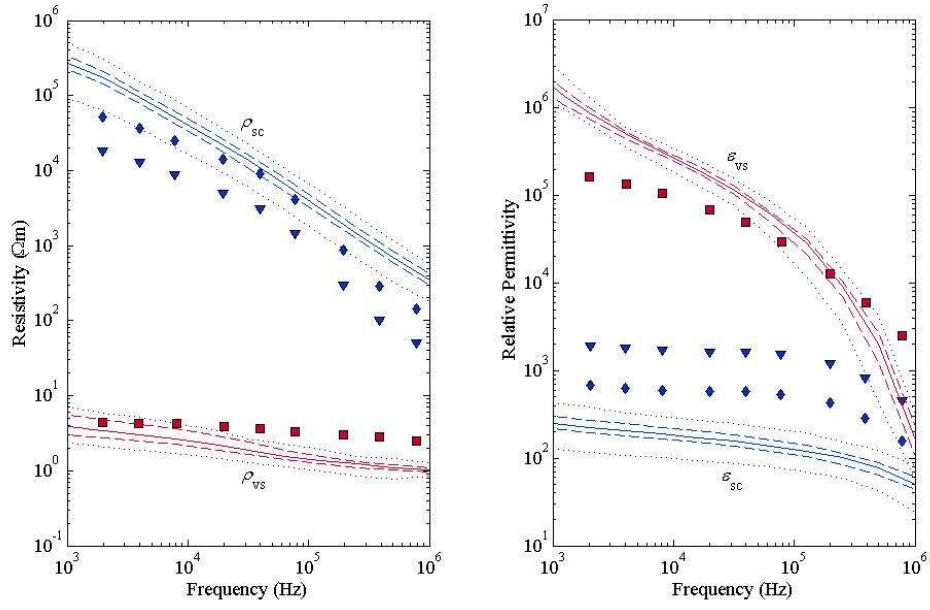


Figure 27 – (a) Estimated resistivity and (b) relative permittivity from the proposed methodology of viable skin and stratum corneum with lower/upper whiskers based on the 1.5 interquartile range ( $\cdots$ ), 25/75th percentiles ( $---$ ) and median ( $—$ ) and (a) average resistivities and (b) permittivity of the ( $\blacktriangledown$ ) stratum corneum by Yamamoto et al., ( $\blacklozenge$ ) adjusted stratum corneum by Birgersson et al., and ( $\blacksquare$ ) viable skin by Yamamoto et al..

## 8.5 STUDY V

In Study V closed form analytical solutions for the mathematical model of EIS from Study IV is secured. As can be inferred from Figure 28, the analytical solutions are able to capture the magnitude and phase of the EIS in the low to mid frequency range up to around  $10^2$  kHz with an error less than 10%; after  $10^2$  kHz, the error increases rapidly up to around 25% and 40% for the magnitude and phase respectively.

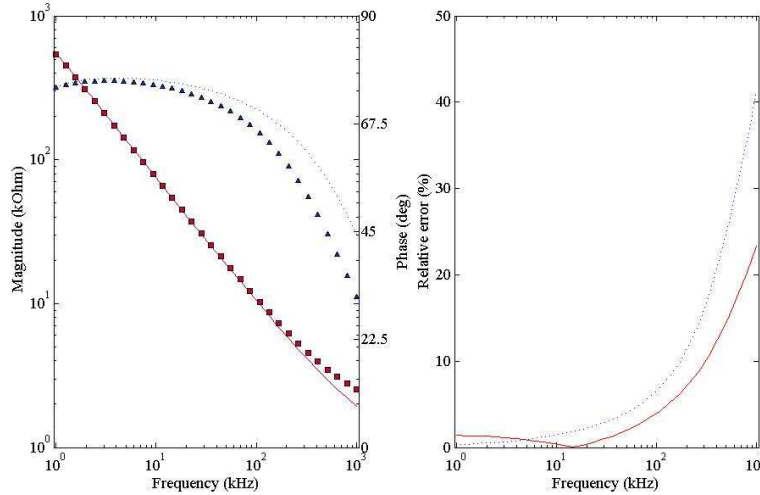


Figure 28 – (a) The magnitude (■) and phase (▲) from the numerical solution of the full set of equations and the analytical counterparts (lines); (b) the relative error for the analytical solution relative to the full set of equations for the magnitude (—) and phase (---).

The main causes for the increasing error with increasing frequency can be found in the underlying assumptions of the Ansatz: first, the assumption that the electrical impedance is dominated by the stratum corneum whilst the viable skin and subcutaneous fat are negligible becomes less accurate with increasing frequency, because it is well known that the impedance of the skin is governed by the stratum corneum only at lower frequencies whilst its influence decreases when the frequency increases [28-31]; this was also demonstrated in the earlier scaling analysis. Second, the assumption that the currents pass straight through the stratum corneum is reasonable in the low- to mid-frequency range; at higher frequencies, however, the current density distributions underneath the electrodes become increasingly more non-uniform and thereby alter the active area of the electrodes. Third, the assumption that the voltage drop will not occur solely over the stratum corneum becomes less accurate with increasing frequency, as was shown earlier with the scales for the potential drops in the scaling analysis around  $10^3$  kHz.

By assuming the stratum corneum thickness to be  $14\text{ }\mu\text{m}$ , we are able to estimate the resistivity and the relative permittivity for each individual subject separately. As can be inferred from Figure 29, the closed form analytical expressions follow the numerical counterparts up to around  $10^2$  kHz, after which the relative permittivity starts to deviate whilst the resistivity agrees throughout the frequency range

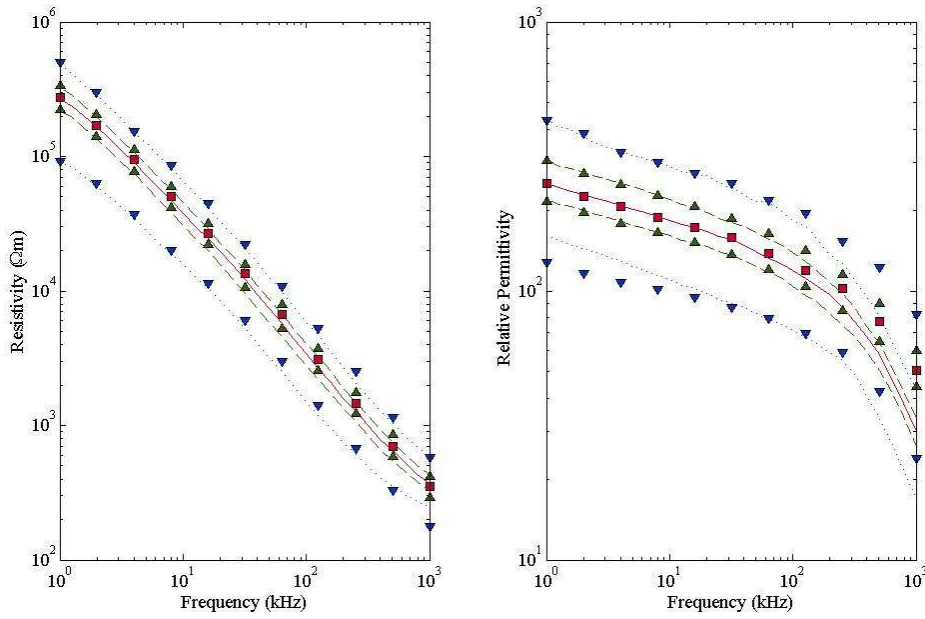


Figure 29 – The median predicted (a) resistivity and (b) relative permittivity for the full set of equations (■) with  $\pm 1$  standard deviation (▲),  $\pm 2$  standard deviations (▼) and the closed-form expressions (—) with  $\pm 1$  standard deviation (---),  $\pm 2$  standard deviations (···)

Finally, we estimate the thickness of the stratum corneum with closed form analytical solutions, by assuming that the material properties are known. As illustrated in Figure 30, the stratum corneum thickness estimate based on the real part of the impedance overestimates the skin thickness slightly, whilst the imaginary part underestimates the skin thickness somewhat; their combination, however, gives rise to an accurate distribution with 92% of the individuals between 6 and 20  $\mu\text{m}$ , which corresponds well with literature values.

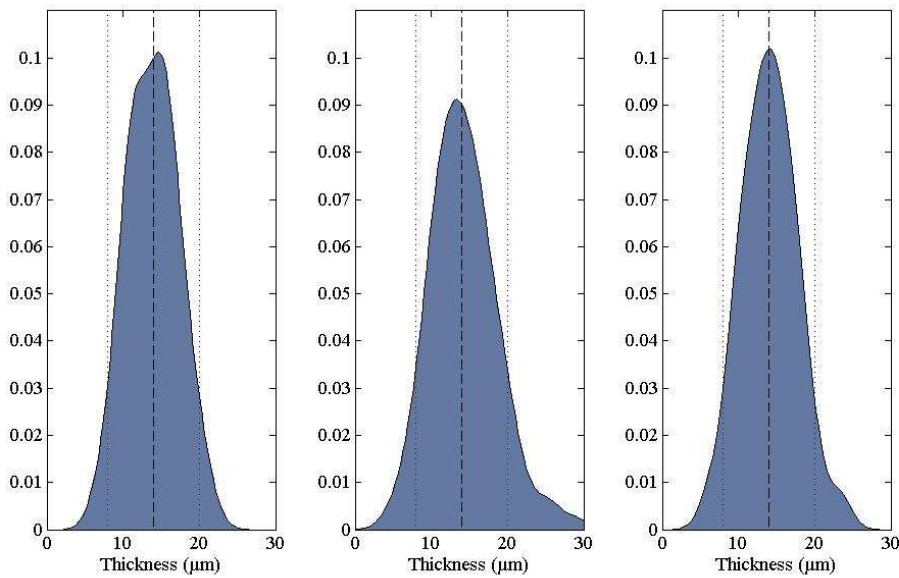


Figure 30 – The estimated thickness distributions for stratum corneum based on the real and imaginary part from EIS measurements and a combination of the two, respectively.

## 9 GENERAL DISCUSSION AND CONCLUSIONS

The overall aim of the studies in this thesis was twofold. The first was oriented in calibrating a classifier in differentiating between malignant melanoma and benign nevi of the skin and evaluating its potential as being utilized as an adjunct diagnostic tool in the clinical decision making whether to excise a lesion or not. The second aim of this thesis was to develop a mathematical model to ascertain the validity of the electrical properties found in literature and to aid in the design and operation of electrodes as well as to broaden the knowledge of the signal distribution in skin.

### 9.1 EFFICACY

The first part of the international melanoma algorithm training study (IMATS) was initiated on the eight of February 2006 with the primary aim to gather at least 150 lesions with histopathologically confirmed diagnosis of malignant melanoma with valid electrical impedance measurements with the purpose of training a classifier in the distinction between benign and malignant cutaneous lesions. The observed accuracy with the SciBase II was significant, but not high enough for a stand-alone decision support tool for the detection of malignant melanomas. Therefore, the study was halted on the first of November 2007 and the SciBase II was upgraded to the SciBase III electrical impedance spectrometer, having a multitude of improvements to come to terms with the limited sensitivity observed in the first part of the study, see section 8.1. The following upgrades were implemented to improve the sensitivity of the device to melanoma:

- 5 bar electrode instead of a 3 bar, with the purpose to increasing the sensitivity field underneath the electrode for small lesions and very early melanoma.
- 10 selectable volume settings instead of the previous 5
- Change of manufacturing process from a silicon (Si) spike-based electrode to a plastic-based production. The upgrade was made due to two main reasons; one being the regulatory issues coupled with spike breakage, as Si is a brittle material, and the second was related to general production issues.
- Spring loaded probe for a fixed applied pressure, to minimize the operator dependency
- Noise reduction, by increasing the applied voltage from 50mV to 250 mV

On the 8 of January 2009, after approximately 1 year, the study could be re-initiated with both updated hardware and redesigned probe and electrode. The last subject was included on the 18 of May 2010 and the final histopathology evaluation was conducted the 18 November 2010.

One of the lessons learnt here was that it is crucial to select a sufficient amount of sites, suitable site locations to ensure the inclusion of lesion and subjects that span the full problem/solution domain by considering the sites referral populations as well as taking into account that the estimates on inclusion can vary significantly, especially in view of the inclusion and exclusion criteria set.

The observed sensitivity in the second part of the IMATS met the aim of 98%, albeit fell just short on the 20 percentage points higher specificity than the clinical diagnosis of dermatologists. The reason is primarily twofold: First, the participating dermatologists were highly experienced in diagnosing cutaneous tumors with the naked-eye and by dermatoscopy, and as such their diagnostic accuracy might have been higher than that of the average dermatologist [63, 68, 104-106]. Secondly, the majority of the lesions included in this study had been suspicious for melanoma and were destined for excision, which is why the clinical sensitivity and specificity, by study design, is 100% and 0% respectively. However, the true clinical specificity in this trial could be considered to fall somewhere between 0% and 8.4%, because a few lesions with a low probability for melanoma had been included.

## **9.2 REQUIREMENTS AND CONSIDERATION FOR ADJUNCT DIAGNOSTIC USAGE**

So far, all results in this study have been presented with a dichotomous outcome. An important consideration in this context is whether the method will be used as an adjunct diagnostic tool or as the diagnostic tool. The Food and Drug Administration (FDA – Regulatory authority in the US) has defined that whenever a test result can over-rule a pre-test clinical result, and the test outcome can function as a stand-alone test, i.e. it does not only provide additional information, it is to be considered as a diagnostic test [107]. Is then a method with a dichotomous outcome by definition a diagnostic test? Given that an adjunct diagnostic test is meant to provide additional information that in combination with the clinical judgment should generate a final clinical diagnosis, the question can clearly be answered with yes. Whenever a positive (1) or negative (0) test result over-rules the pre-test clinical diagnosis, it is by this definition diagnostic, even though the information given just tends to tip the balance of the clinical diagnosis. One way to conform to the regulatory requirements for an adjunct diagnostic tool could be to incorporate a score output, e.g. 0-10 where 0 is considered as benign and 10 as malignant. This would provide additional information rather than a dichotomous outcome, which always can be viewed as a stand-alone test. An alternative approach to incorporate a score could be to give the clinician the possibility to adjust the cut-off for the dichotomous outcome, thus potentially making the method adjunctive rather than purely diagnostic, as it can no longer be considered as a truly stand-alone test.

Once all the above considerations have been taken into account, a final consideration still needs to be addressed regarding the intended use of the method, i.e. in what situations can clinical value be proven.

In conclusion, EIS has the potential to be used as an adjunct diagnostic tool to help clinicians differentiate between benign and malignant cutaneous lesions, although further studies were needed to confirm the validity of the classification algorithm. Therefore the SciBase International Melanoma Pivotal Trial (SIMPS) was initiated in 2010 to evaluate the safety and efficacy of the SciBase III system, including derived classifier on a fully blinded test set.

### 9.3 MATHEMATICAL MODELING AND ELECTRICAL PROPERTIES OF SKIN

In Study III, a mathematical model of the skin considering conservation of charge was derived and experimentally validated. The findings led to an adjustment of the average resistivity and relative permittivity of the stratum corneum derived earlier by Yamamoto and Yamamoto [27]. By adjusting the dielectrical properties, a good agreement between the model predictions and experimental findings after application of an 18% sodium chloride solution for 30 min was achieved; however, when physiological saline solution is employed as a moisturizer, the model predictions were less accurate. Hence there was a need for further improvements to determine more accurate dielectrical properties of the stratum corneum and the underlying viable skin, and by accounting for a more accurate skin thickness, nonlinearity of the stripping technique, heterogeneity of the skin layers, cohort size, ion concentration of the moisturizer as well as the soaking time.

The findings show that the measured impedance is modulated by the applied solvent and soaking time; it is thus essential that the electrical properties of the skin are presented in this context.

In Study IV, a methodology based on experimental impedance measurements, a mathematical model comprising conservation of charge in the functional layers of human skin coupled with automated code generation and an optimization algorithm was developed and verified experimentally. More accurate resistivity and permittivity values for viable skin and stratum corneum soaked with a physiological saline solution for 1 minute on the volar forearm were obtained and expressed as easily accessible functions.

The therein presented methodology can be extended to encompass other types of tissue, soaking time, and different solvents, which in turn allows for extraction of new electrical material properties as well as analysis of the current and voltage distributions. In addition, the methodology can be extended to study electrode design, coupled physical phenomena such as deformation of the skin during impedance measurements, and by increasing the spatial resolution of the skin enhance the information of distribution of the signal, and of course to other clinical changes.

In Study V, closed-form analytical expressions were derived in the limit of low frequencies around 1 kHz. Their accuracy and region of validity were found to be 1 kHz to around  $10^2$  kHz from the verification of the full set of equations solved numerically as well as validation with experimentally measured impedances at different depth settings from a total of 120 subjects. By combining experimental impedance measurements with the analytical expressions, the electrical properties of the stratum corneum (provided the stratum corneum thickness is known) but also its thickness could be estimated. This suggests that EIS could be employed as a method to estimate the stratum corneum thickness at 1 kHz; its suitability ought to be further validated by

carrying out EIS measurements in tandem with one or several techniques to measure the stratum corneum thickness (see Section 7.2) to establish that one is indeed measuring a reasonably “true” thickness of the stratum corneum for each subject and not just the distribution.

## 10 FUTURE STUDIES

### 10.1 CLINICAL STUDIES

First and foremost a study to confirm the validity of the classification algorithm described in Study II is necessary. This study was initiated in 2010 and as of today the study is finalized and the database is locked [108]. The statistical analysis is currently being performed and results are planned to be published in a peer-review journal during 2013.

Once the study efficacy and safety have been analyzed and found to be sufficient to market the device, at least two studies will be necessary. Firstly, the clinical utility of the device needs to be determined, i.e. how is the device going to be used in clinical praxis? Secondly, there are numerous health economic studies that need to be conducted in conjunction with determining the clinical utility to obtain reimbursement for a medical device. Since the health economic systems are most often country specific, one health economic study will not be sufficient to answer the question if the device provides any health economic values in other countries.

In the pivotal trial, all lesions were photo documented and all histopathology slides were scanned and reviewed by both a local histopathologist and a board consisting of 3-5 histopathologists. This database enables a number of possible studies to be conducted, such as the analysis of the general discordance between histopathologist. Is the discordance based only on difference in the melanoma pattern recognitions or are there other influencing factors that should be taken into account, such as the quality of the slide preparation? Are there any country specific differences? Furthermore, the material can also be used for teaching purposes where the visual interpretation of a lesion is combined with histopathology.

The derived methodology in Study IV can be extended into numerous studies to study electrode design, coupled physical phenomena such as deformation of the skin in combination with impedance measurement, increasing the resolution of the skin (for example extending the model to incorporate the latest findings of Iwai et al. [109]), water gradient analysis as well as other clinical changes.

In addition, carrying out EIS measurements in tandem with one or several techniques to measure the skin thickness would determine the “true” variability of the electrical properties of the stratum corneum and viable skin by opening up the possibility to incorporate the actual skin thickness in the calibration. Moreover, the estimates of the stratum corneum thickness could also be validated on individual-level rather than on a population-level.

## 11 ACKNOWLEDGEMENTS

I wish to express my genuine gratitude to:

**Stig Ollmar**, my main supervisor, for keeping me on track, enthusiastic encouragement and generous support throughout this thesis.

**Johan Hansson** and **Jan Bolinder**, my clinical supervisors, for lending a hand whenever the need arose.

**Erik Birgersson**, for guidance in the field of mathematical modeling, fruitful discussions and not the least in helping me sort out the good ideas from the bad.

**Peter Åberg**, for productive collaboration and guiding me in the early stages of this thesis.

**Ingrid Nicander**, for her collaboration and providing me with much needed clinical data.

All **investigators**, **study nurses**, **histopathologist** and **co-authors** who have been involved in either the design of the research studies, conducted the actual measurements or helped in the finalization of the papers. I am especially grateful for all fruitful discussions on the topic of skin cancer.

**Annika Ternesten-Bratel**, **Karen Blessing** and **Mecislovas Simanaitis**, for working thorough the enormous amount of histopathology slides and for still being able to take time out of their extremely busy schedules to help in the interpretation of the histopathology findings.

To all my colleagues, both former and present at **SciBase AB**, for creating a welcoming atmosphere and productive environment. Special thanks goes to **Anders Lundqvist** for making it possible to combine a scientific as well as industrial growth, to **Per Svedenhag** for always providing good insights, to **Annika Solehav** for enthusiastically pushing me on and not the least, to **Lena Melltorn** for always keeping a stack of papers to allow me, quite literally, to draw the outlines of my ideas to test their validity, especially on late Friday afternoons.

I would like to thank the people at **CLINTEC** for providing a helpful and friendly working environment.

Finally, I would like to extend my deepest gratitude to my **father** and **mother** for investing so much time, money and effort in my life and education. A warm gratitude goes to my **brothers**, for not letting me get away with *just* a Master of Science.

*Stockholm, 10<sup>th</sup> of December 2012*

*Ulrik Birgersson*

## 12 REFERENCES

1. Grimnes S, Martinsen Ø. Bioimpedance and bioelectricity basics. London (UK): Academic Press, 2000.
2. Ollmar S, Nicander I. Within and beyond the skin barrier. In Bioengineering of the skin - Water and the stratum corneum, 2nd ed., pp 335-350. Fluhr, Elsner, Berardesca, Maibach (Eds.). CRC Press 2005.
3. Emtestam L, Nicander I, Stenström M, Ollmar S. Electrical impedance of nodular basal cell carcinoma: a pilot study. *Dermatology* 1998; vol. 197: 313-316.
4. Åberg P, Nicander I, Holmgren U, Geladi P, Ollmar S. Assessment of skin lesions and skin cancer using simple electrical impedance indices. *Skin Res Technol* 2003; vol. 9: 257-261.
5. Beetner DG, Kapoor S, Manjunath S, Zhou X, Stoecker W. Differentiation among basal cell carcinoma, benign lesions, and normal skin using electrical impedance. *IEEE Trans Biomed Eng* 2003; vol. 50: 1020-1025.
6. Åberg P, Nicander I, Holmgren U, Hansson J, Ollmar S. Bioimpedance as a potential diagnostic decision tool for skin neoplasms. In Proc. EMBEC'02, Vienna, Dec. 2002, vol. 3, pp. 80-81.
7. Dua R, Beetner DG, Stoecker WV, Wunsch DC 2nd. Detection of basal cell carcinoma using electrical impedance and neural networks. *IEEE Trans Biomed Eng* 2004; 51(1): 66-71.
8. Åberg P, Nicander I, Hansson J, Geladi P, Holmgren U, Ollmar S. Skin cancer identification using multi-frequency electrical impedance – a potential screening tool. *IEEE Trans Biomed Eng* 2004; 51(12):2097- 2102.
9. Åberg P, Nicander I, Ollmar S. Minimally invasive electrical impedance spectroscopy of skin exemplified by skin cancer assessments. In Proc. IEEE EMBS'03, Cancun (MX), pp. 3211-3214, Sep. 2003.
10. Åberg P, Geladi P, Nicander I, Hansson J, Holmgren U, Ollmar S. Non-invasive and microinvasive electrical impedance spectra of skin cancer - a comparison between two techniques. *Skin Res Technol* 2005; vol 11: 281-6.
11. Grahm-Brown R, Bourke J. Mosby's Color Atlas and Text of Dermatology, 2<sup>nd</sup> edition Elsevier Limited, 2007.
12. Hunter J.A.A, Saving J.A, Dahl M.V, Clinical Dermatology, 3<sup>rd</sup> edition, Wiley-Blackwell 2002.
13. Meredith P, Riesz J. Radiative relaxation quantum yields for synthetic eumelanin. *Photochemistry and photobiology* 2004; 79 vol. 2: 211–6
14. Rorsman H, Björnberg A, Vahlquist A. *Dermatologi Venerologi*, Studentlitteratur, 2000.
15. Schwan H P. Electrical properties of tissue and cell suspensions. *Advances in biological and medical physics* 1957; vol. 5: 147-224.
16. Cole K and Cole R. Dispersion and absorption in dielectrics. I: alternating current characteristics *J. Chem. Phys.* 1941; 9: 341–51.
17. Foster K R, Schwan H P. Dielectric-Properties of Tissues and Biological-Materials-a Critical Review. *Critical Reviews in Biomedical Engineering* vol. 17, pp 25-104, 1989.
18. Gabriel S, Lau R W and Gabriel C. The dielectric properties of biological tissue: II. Measurements in the frequency range 10 Hz to 20 GHz. *Phys. Med. Biol.* 1996; 41: 2251–69.

19. Jones D M, Smallwood R H, Hose D R, Brown B H and Walker D C. Modelling of epithelial tissue impedance measured using three different design of probe *Physiol. Meas.* 2003; 24: 605–23
20. Keshtkar A, Keshtkar A and Smallwood R H. Electrical impedance spectroscopy and the diagnosis of bladder pathology. *Physiol. Meas.* 2006; 27: 586–96
21. Balasubramani L, Brown B H, Healey J and Tidy J A. The detection of cervical intraepithelial neoplasia by electrical impedance spectroscopy: the effects of acetic acid and tissue homogeneity. *Gynecol. Oncol.* 2009; 115: 267–71
22. Walker D C, Brown B H, Blackett A D, Tidy J and Smallwood R H. A study of the morphological parameters of cervical squamous epithelium *Physiol. Meas.* 2003; 24: 121–35
23. Walker D C, Brown B H, Smallwood R H, Hose D R and Jones D M. Modelled current distribution in cervical squamous carcinoma. *Physiol. Meas.* 2002; 23: 159–68
24. Walker D C, Brown B H, Smallwood R H, Hose D R and Jones D M. Modelling the electrical properties of bladder tissue—quantifying impedance changes due to inflammation and oedema. *Physiol. Meas.* 2005; 26: 251–68
25. Brown B H. Electrical impedance tomography (EIT): a review. *J Med Eng Technol*, 2003; vol. 27: 387-393
26. Ellis K J. Human Body Composition: In Vivo Methods. *Physiological Reviews.* 2000; Vol 80 (2): 649-680
27. Yamamoto T and Yamamoto Y. Electrical properties of the epidermal stratum corneum *Med. Biol. Eng.* 1976; 14: 151–8
28. Ackmann J J and Seitz M A. Methods of complex impedance measurements in biologic tissue *Crit. Rev. Biomed. Eng.* 1984; 11: 281–311
29. Martinsen OG, Grimnes S, Haug E. Measuring depth depends on frequency in electrical skin impedance measurements. *Skin Res Technol.* 1999; 5: 179-181.
30. Birgersson U, Birgersson E, Åberg P, Nicander I, Ollmar S. Non-invasive bioimpedance of intact skin: mathematical modeling and experiments. *Physiol. Meas.* 2011; 32: 1-18.
31. Birgersson U, Birgersson E, Nicander I, Ollmar S. A methodology for extracting the electrical properties of human skin. Manuscript submitted for publication in *Physiol. Meas.* 2012.
32. Birgersson U, Birgersson E, Ollmar S. Estimating electrical properties and the thickness of skin with electrical impedance spectroscopy: Mathematical analysis and measurements. *J Electr Bioimp*, 2012; vol. 3: 51–60.
33. Nicander I, Ollmar S, Eek A, Lundh Rozell B, Emtestam L. Correlation of impedance response patterns to histological findings in irritant skin reactions induced by various surfactants. *Br J Dermatol* 1996; vol. 134: 221-8.
34. Nicander I, Ollmar S. Mild and below threshold skin responses to sodium lauryl sulphate assessed by depth controlled electrical impedance. *Skin Res Technol* 1997; vol. 3: 259-263.
35. Nyren M, Hagstromer L, Emtestam L. Instrumental measurement of the Mantoux test: differential effects of tuberculin and sodium lauryl sulphate on impedance response patterns in human skin. *Dermatology* 2000; vol. 201: 212-7.
36. Nicander I, Åberg P, Ollmar S. The use of different concentrations of betaine as a reducing irritation agent in soaps monitored visually and non-invasively. *Skin Res Technol* 2003; vol. 9: 43-9.

37. Nicander I, Rantanen I, Lundh Rozell B, Soderling E, Ollmar S. The ability of betaine to reduce the irritating effects of detergents assessed visually, histologically and by bioengineering methods. *Skin Res Technol* 2003; vol. 9: 50-8.
38. Nicander I, Ollmar S. Clinically normal atopic skin vs. nonatopic skin as seen through electrical impedance. *Skin Res Technol* 2004; vol. 10: 178-83.
39. Lindholm-Sethson B, Han S, Ollmar S, Nicander I, Jonsson G, Lithner F, Bertheim U, Geladi P. Multivariate analysis of skin impedance data in long-term type 1 diabetic patients. *Chemometrics and Intelligent Laboratory Systems* 1998; vol. 44: 381-394.
40. Nicander I. Electrical impedance related to experimentally induced changes of human skin and oral mucosa (PhD thesis). Karolinska Institutet, Stockholm, Sweden, 1998.
41. Tsao H, Sober A. Acquired precursor lesions and markers of increased risk for cutaneous melanoma. In: Balch C, Houghton A, Sober A, Soong S, eds. *Cutaneous melanoma*. 4th ed. St. Louis: Quality Medical Publishing 2003: 121-34.
42. Tsao H, Bevona C, Goggins W, Quinn T. The transformation rate of moles (melanocytic nevi) into cutaneous melanoma: a population-based estimate. *Arch Dermatol* 2003; 139: 282-8.
43. Elwood JM, Jopson J. Melanoma and sun exposure: an overview of published studies. *Int J Cancer* 1997; 73: 198-203.
44. Tsao H, Sober AJ. Ultraviolet radiation and malignant melanoma. *Clin Dermatol* 1998; 16: 67-73.
45. Kang S, Barnhill RL, Mihm MC Jr, Sober AJ. Multiple primary cutaneous melanomas. *Cancer* 1992; 70: 1911-6.
46. Goggins WB, Tsao H. A populationbased analysis of risk factors for a second primary cutaneous melanoma among melanoma survivors. *Cancer* 2003; 97: 639-43.
47. Clark WH Jr, Reimer RR, Greene M, Ainsworth AM, Mastrangelo MJ. Origin of familial malignant melanomas from heritable melanocytic lesions: the 'B-K mole syndrome.' *Arch Dermatol* 1978; 114: 732-8.
48. Lynch HT, Fritchot BC III, Lynch JF. Familial atypical multiple mole-melanoma syndrome. *J Med Genet* 1978; 15: 352-6.
49. NIH Consensus Conference: diagnosis and treatment of early melanoma. *JAMA* 1992; 268: 1314-9.
50. Kraemer KH, Tucker M, Tarone R, Elder DE, Clark WH Jr. Risk of cutaneous melanoma in dysplastic nevus syndrome types A and B. *N Engl J Med* 1986; 315: 1615-6.
51. Greene MH, Clark WH Jr, Tucker MA, Kraemer KH, Elder DE, Fraser MC. High risk of malignant melanoma in melanomaprone families with dysplastic nevi. *Ann Intern Med* 1985; 102: 458-65.
52. Bishop DT, Demenais F, Goldstein AM, et al. Geographical variation in the penetrance of CDKN2A mutations for melanoma. *J Natl Cancer Inst* 2002; 94: 894-903.
53. National Cancer Institute. SEER cancer statistics.(Accessed in 2010, at <http://seer.cancer.gov>)
54. International Agency for Research on Cancer. (Accessed in 2012, at <http://globocan.iarc.fr/>)
55. Balch C M, Gershenwald J E, Soong S-J, Thompson J F et al. Final Version of 2009 AJCC Melanoma Staging and Classification. *Journal of Clinical Oncology* 2009; vol 27: (36).

56. Tsao H, Atkins M B, Sober A J. Management of Cutaneous Melanoma. The new England journal of Medicine 2004; 351 (10): 998-1012
57. Madan V, Lear J T, Szeimies R-M. Non-melanoma skin cancer. Lancet 2010; vol. 375: 673-85
58. American Academy of Dermatology. (Accessed in 2012 <http://www.aad.org/media-resources/stats-and-facts/conditions/skin-cancer>)
59. Aberg P. Skin cancer as seen by electrical impedance. PhD Thesis, Karolinska Institutet, Stockholm, Sweden, 2004
60. SciBase 2012 SciBase AB Homepage <http://www.scibase.se>
61. Davis N. Modern concepts of melanoma and its management. Ann Plast Surg 1978; 1: 628-629.
62. Abbasi R N, Shaw M H, Rigel S D, Friedman J R et al. Early Diagnosis of Cutaneous Melanoma. Revisiting the ABCD Criteria. JAMA 2004; 292(22): 2771-76.
63. Kittler H, Pehamberger H, Wolff K, Binder M. Diagnostic accuracy of dermoscopy. Lancet Oncol 2002; 3 (3): 159–165.
64. Stolz W, Riemann A, Cagnetta AB, et al. ABCD rule of dermoscopy: a new practical method for early recognition of malignant melanoma. Eur J Dermatol 1994; 4: 521-7
65. Menzies SW. A method for the diagnosis of primary cutaneous melanoma using surface microscopy. Dermatol Clin 2001; 19: 171-6.
66. Argenziano G, Fabbrocini G, Carli P, et al. Epiluminescence microscopy for the diagnosis of doubtful melanocytic lesions: Comparison of the ABCD rule of dermoscopy and a new 7-point checklist based on pattern analysis. Arch Dermatol 1998; 134: 1563-1570
67. Byrnes P, Ackermann E, Williams ID, Mitchell GK, Askew D. Management of skin cancer in Australia--a comparison of general practice and skin cancer clinics. Aust Fam Physician. 2007; 36 (12): 1073-5.
68. Carli P, De Giorgi V, Crocetti E, Mannone F, Massi D, Chiarugi A, Giannotti B. Improvement of malignant/benign ratio in excised melanocytic lesions in the 'dermoscopy era': a retrospective study 1997-2001. Br J Dermatol 2004; 150 (4): 687-92.
69. English DR, Burton RC, del Mar CB, Donovan RJ, Ireland PD, Emery G. Evaluation of aid to diagnosis of pigmented skin lesions in general practice: controlled trial randomised by practice. BMJ 2003; 327: 1-6.
70. Menzies SW, Emery J, Staples M, Davies S, McAvoy B, Fletcher J, Shahid KR, Reid G, Avramidis M, Ward AM, Burton RC, Elwood JM. Impact of dermoscopy and short-term sequential digital dermoscopy imaging for the management of pigmented lesions in primary care: a sequential intervention trial. Br J Dermatol 2009; 161 (6): 1270-7.
71. Soares TF, Laman SD, Yiannias JA, Connolly SM, Lim KK, Wu Q, Swanson DL. Factors leading to the biopsy of 1547 pigmented lesions at Mayo Clinic, Scottsdale, Arizona, in 2005. Int J Dermatol 2009; 48 (10): 1053-6.
72. Guitera P, Menzies S. State of the art of diagnostic technology for early-stage melanoma. Expert Reviews 2011: 715-723
73. Farmer E R, Gonin R, Hanna M P. Discordance in the Histopathologic Diagnosis of Melanoma and Melanocytic Nevi Between Expert Pathologists Hum Pathol 1996; 27: 528–531.
74. Soyer P, Massone C, Ferrara G, Argenziano G. Limitations of histopathologic analysis in the recognition of melanoma: a plea for a combined diagnostic approach of histopathologic and dermoscopic evaluation. Arch Dermatol 2005; 141: 209–211.

75. Lodha S, Saggar S, Celebi J, Silvers D. Discordance in the histopathologic diagnosis of difficult melanocytic neoplasms in the clinical setting. *J Cutan Pathol* 2008; 35: 349–352.
76. Braun R P, Gutkowitz-Krusin D, Rabinovitz H, Coggnetta A. Agreement of Dermatopathologists in the Evaluation of Clinically Difficult Melanocytic Lesions: How Golden Is the ‘Gold Standard’? *Dermatology* 2012; 224: 51–58
77. Pearson K. On lines and planes of closest fit to systems of points in space. *Philosophical Magazine* 1901; vol. 2: 559-572.
78. Nyström J, Lindholm-Sethson B, Stenberg L, Ollmar S, Eriksson JW, Geladi P. Combined near-infrared spectroscopy and multifrequency bio-impedance investigation of skin alterations in diabetes patients based on multivariate analyses. *Med Biol Eng Comput* 2003; vol. 41: 324-9.
79. Eriksson L, Johansson E, Kettaneh-Wold N, Trygg J et al. Multi- and Megavariate Data Analysis Part I, 2<sup>nd</sup> revision. Umetrics AB 2006.
80. Scholkopf B, Smola A. Learning with Kernels. Cambridge Massachusetts: MIT Press , 2002.
81. Lee TK and Claridge E. Predictive power of irregular border shapes for malignant melanomas. *Skin Res Technol* 2005; 11: 1-8.
82. Hanley JA, McNeil BJ. The meaning and use of the area under a receiver operating characteristic (ROC) curve. *Radiology* 1982; vol. 143: 29-36
83. Brown BH, Tidy JA, Boston K, Blackett AD, Smallwood RH, Sharp F. Relation between tissue structure and imposed electrical current flow in cervical neoplasia. *Lancet* 2000; vol. 355: 892-895
84. Smallwood R, Hamdy F, Keshtkar A, Wilkinson B, Lee J, Azzouzi R. Electrical impedance spectroscopy identifies malignant areas in the bladder. In proc. XII Intern Conf on Electrical Bio-Impedance & V Electrical Impedance Tomography, Gdansk (PL), pp. 425-428, 2004. ISBN 83-917681-6-3.
85. Tronstad C, Gjein G E, Grimnes S, Martinsen OG, Krogstad AL, Fosse E. Electrical measurement of sweat activity. *Physiol. Meas.* 2008; 29: 407–15
86. Norlen L, Plasencia I, Bagatolli L. Stratum corneum lipid organization as observed by atomic force, confocal and two-photon excitation fluorescence microscopy *Int. J. Cosmet. Sci.* 2008; 30: 391–411
87. Tsukahara K, Takema Y, Moriwaki S, Fujimura T and Imokawa G. Dermal fluid translocation is an important determinant of the diurnal variation in human skin thickness *Br. J. Dermatol.* 2001; 145: 590–6
88. Hartinger A E, Guardo R, Kokta V and Gagnon H. A 3D hybrid finite element model to characterize the electrical behavior of cutaneous tissues *IEEE Trans. Biomed. Eng.* 2010; 57: 780–9
89. Egawa M, Hirao T and Takahashi M. In vivo estimation of stratum corneum thickness from water concentration profiles obtained with Raman spectroscopy. *Acta Derm. Venereol.* 2007; 87: 4–8
90. Egawa M and Tagami H. Comparison of the depth profiles of water and water-binding substances in the stratum corneum determined in vivo by Raman spectroscopy between the cheek and volar forearm skin: effects of age, seasonal changes and artificial forced hydration *Br. J. Dermatol.* 2008; 158: 251–60
91. Crowther JM, Sieg A, Blenkiron P, Marcott C, Matts PJ, Kaczvinsky JR, Rawlings AV. Measuring the effects of topical moisturizers on changes in stratum corneum thickness, water gradients and hydration in vivo *Br. J. Dermatol.* 2008; 159: 567–77

92. Huzaira M, Rius F, Rajadhyaksha M, Anderson RR and Gonzales S. Topographic variations in normal skin, as viewed by in vivo reflectance confocal microscopy. *J. Invest. Dermatol.* 2001; 116: 846–52.
93. Hoffmann K, Stucker M, Dirschka T, Gortz S, El Gammal S, Dirting K, Hoffmann A, Altmeyer P. Twenty MHz B-scan sonography for visualization and skin thickness measurement of human skin *J. Eur. Acad. Dermatol. Venereol.* 1994; 3: 302–13
94. Seidenari S, Giusti G, Bertoni L, Magnoni C, Pellacani G. Thickness and echogenicity of the skin in children assessed by 20-MHz ultrasound *Dermatology* 2000; 201: 218–22
95. Moore T L, Lunt M, McManus B, Anderson M E and Herrick A L. Seventeen-point dermal ultrasound scoring system-a reliable measure of skin thickness in patients with systemic sclerosis *Rheumatology* 2003; 42: 1559–63
96. Sandby-Moller J, Poulsen T and Wulf H C. Epidermal thickness at different body sites: relationship to age, gender, pigmentation, blood content, skin type and smoking habits. *Acta Derm. Venereol.* 2003; 83: 410–3
97. Holbrook K and Odland G. Regional differences in the thickness (cell layers) of the human stratum corneum: an ultrastructural analysis *J. Invest. Dermatol.* 1974; 62: 415–22
98. Schwindt D A, Wilhelm K P and Maibach H I. Water diffusion characteristics of human stratum corneum at different anatomical sites in vivo. *J. Invest. Dermatol.* 1998; 111: 385–9
99. Pirot F, Berardesca E, Kalia Y N, Singh M, Maibach H I, Guy R H. Stratum corneum thickness and apparent water diffusivity: facile and noninvasive quantitation in vivo *Pharm. Res.* 1998; 15: 492–4
100. Tsai J C, Lin C Y, Sheu H M, Lo Y L and Huang Y H. Noninvasive characterization of regional variation in drug transport into human stratum corneum in vivo *Pharma. Res.* 2003; 20: 632–8
101. Bedard C, Kroger H, Destexhe A. Modeling extracellular field potentials and the frequency-filtering properties of extracellular space *Biophys. J.* 2004; 86: 1829–42
102. Miller C E, Henriquez C S. Finite element analysis of bioelectric phenomena *Crit. Rev. Biomed. Eng.* 1990; 18: 207–33
103. Gabriel S, Lau R W, and Gabriel C. The dielectric properties of biological tissue: II. Measurements in the frequency range 10 Hz to 20 GHz. *Phys. Med. Biol.* 1996; 41: 2251–69
104. Soyer HP, Smolle J, Hödl S, Pachernegg H, Kerl H. Surface microscopy. A new approach to the diagnosis of cutaneous pigmented tumors. *Am J Dermatopathology* 1989; 11: 1-10.
105. Piccolo D, Ferrari A, Peris K, Diadone R, Ruggeri B, Chimenti S. Dermoscopic Diagnosis by a trained clinician vs. a clinician with minimal dermoscopy training vs. computer-aided diagnosis of 341 pigmented skin lesions: a comparative study. *Br J Dermatol* 2002; 147: 481-486.
106. Vestergaard ME, Macaskill P, Holt PE, Menzies SW. Dermoscopy compared with naked eye examination for the diagnosis of primary melanoma: a meta-analysis of studies performed in a clinical setting. *Br J Dermatol* 2008; 159: 669-676.
107. FDA 2012, U.S. Food and Drug Administration, difference between diagnostic and adjunct diagnostic test.  
<http://www.fda.gov/downloads/AdvisoryCommittees/CommitteesMeetingMat>

erials/MedicalDevices/MedicalDevicesAdvisoryCommittee/GeneralandPlastic  
SurgeryDevicesPanel/UCM263807.pdf

108. ClinicalTrials.gov. (Accessed December 2012).  
<http://www.clinicaltrials.gov/ct2/show/NCT01077050?term=SciBase+International+Melanoma+Pivotal+Trial&rank=1>
109. Iwai I, Han H, den Hollander L, Svensson S., Öfverstedt L, Anwar J, Brewer J., Bloksgaard M, Laloëuf A, Nosek D. et al. The human skin barrier is organized as stacked bilayers of fully extended ceramides with cholesterol molecules associated with the ceramide sphingoid moiety. *Journal of Investigative Dermatology* 2012; 132: 2215-2225.